JACS
JOURNAL OF THE AMERICAN CHEMICAL SOCIETY
pubs.acs.org/JACS
Article

Lithiated Oppolzer Enolates: Solution Structures, Mechanism of Alkylation, and Origin of Stereoselectivity

Nathan M. Lui, Samantha N. MacMillan, and David B. Collum*

Cite This: https://doi.org/10.1021/jacs.2c09341
Read Online

ABSTRACT: Camphorsultam-based lithium enolates referred to colloquially as Oppolzer enolates are examined spectroscopically, crystallographically, kinetically, and computationally to ascertain the mechanism of alkylation and the origin of the stereoselectivity. Solvent- and substrate-dependent structures include tetramers for alkyl-substituted enolates in toluene, unsymmetric dimers for aryl-substituted enolates in toluene, substrate-independent symmetric dimers in THF and THF/toluene mixtures, HMPA-bridged trisolvated dimers at low HMPA concentrations, and disolvated monomers for the aryl-substituted enolates at elevated HMPA concentrations. Extensive analyses of the stereochemistry of aggregation are included. Rate studies for reaction with allyl bromide implicate an HMPA-solvated ion pair with a $^{+}Li(HMPA)_4$ counterion. Dependencies on toluene and THF are attributed to exclusively secondary-shell (medium) effects. Aided by density functional theory (DFT) computations, a stereochemical model is presented in which neither chelates nor the lithium gegenion serves roles. The stereoselectivity stems from the chirality within the sultam ring and not the camphor skeletal core.

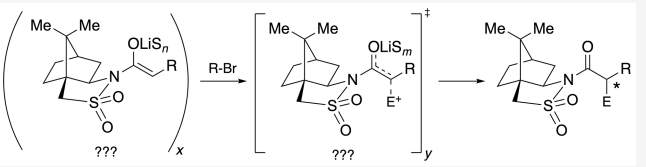

INTRODUCTION

A survey of scaled procedures used by Pfizer Process over two decades showed that 68% of all C−C bond formations were carbanion-based, and *64% of these involved enolates.*[1,2] A survey of over 500 academic natural product syntheses revealed that lithium diisopropylamide (LDA) was the most commonly used reagent, which certainly involved a considerable number of lithium enolates.[3] Thus, the central importance of lithium enolates in organic synthesis is unassailable.[4]

We submit that understanding how solvation and aggregation influence enolate reactivity and selectivity also has a niche, but it has been a particularly challenging problem. During a collaboration with the Sanofi-Aventis process group to study β-amino ester enolates (**1**, Chart 1),[5] we happened upon a generalizable protocol[6] for determining aggregation states of O−Li species in solutions.[7] This initiated studies of structure−reactivity−selectivity relationships of synthetically important enolates ranging from simple to functionally complex (Chart 1).[8]

Chart 1. Synthetically Relevant Enolates Characterized in a Solution[5,8]

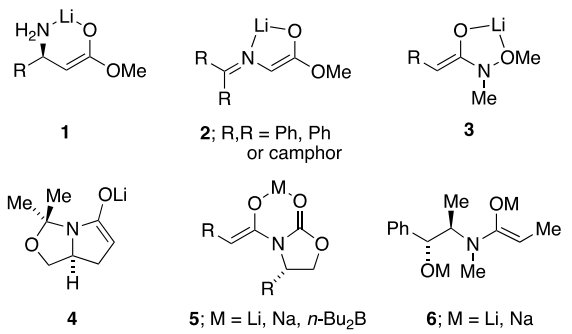

Notably absent from Chart 1 are camphor-based Oppolzer enolates exemplified by lithium enolate **8** in eq 1.[9] Highly stereoselective functionalizations using a range of counterions are attributed to transition structures depicted as **10** in which stereocontrol to form **9** stems from an *endo*-face approach to the sultam-based chelates. We describe herein studies of the lithium enolates of type **8**, exploring how the solvent influences aggregate structure and the mechanism underlying highly stereoselective alkylations. After wading through some strikingly complex aggregation and solvation effects, we found that the sulfonyl-based chelates are structurally important but do *not* influence the stereoselectivity of alkylation. Moreover, neither the lithium counterion nor the camphor methyl moieties influence the stereochemistry. The unglamorous function of the camphor skeleton is to anchor the C−C−C−N dihedral angle in sultam **11**. The sulfonyl moiety plays a key and quite unexpected role.

Received: September 1, 2022

https://doi.org/10.1021/jacs.2c09341
J. Am. Chem. Soc. XXXX, XXX, XXX−XXX

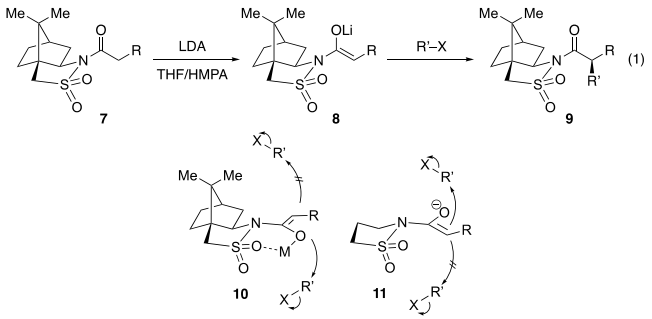

The bulk of the study focuses on the structures of aryl acetamide-derived enolates and their alkylation.[10] Although this is logical given the prevalence of pharmaceutical agents with aryl propionate substructures[11] and considerable room for further development of their syntheses using the Oppolzer enolates,[12] the aryl acetamide-derived enolates are more structurally tractable than their alkyl counterparts. For the casual readers, the Discussion summarizes the solvent-dependent structures and mechanism of alkylation. For the more structurally and mechanistically inclined readers, the Results section details the challenges and methods for determining the solution structure.

Background: Structure Determination. Structure and mechanism are inseparably entwined. In 1968, Edwards *et al.*[13] reduced reaction kinetics to a simple (paraphrased) maxim: the rate law provides the stoichiometry of the transition structure relative to the reactants. It offers the empirical formula of the transition structure *provided the structures of all reactants are known*. Thus, the success of a detailed mechanistic study depends critically on understanding and *controlling* the structures of the reactants. Having determined hundreds of rate laws over decades, however, we can say with confidence that the challenges posed by structural variability in the *reactants* are far more vexing than those arising from multiple *transition structures*.

Seebach, Williard, and others laid important foundations by determining enolate crystal structures showing what *might* exist in solutions.[14] Lithium enolate solution structures, however, were elusive owing to the absence of spin−spin coupling in the O−Li linkage that was central to understanding C−Li and N−Li species.[15−17] Early solution structural studies of enolates employed colligative measurements to obtain *average* molecular weights of all species in solutions inferred from measured solution molalities,[18] but these methods are opaque and error-prone owing to the possibility of complex equilibria and undetected impurities. Diffusion-ordered NMR spectroscopy (DOSY) promoted in organolithium chemistry contemporaneously by Williard *et al.*[19] and Neufeld and Stalke[20] shows great promise by providing relative molecular weights of the independent species. Although questions remain about the contributions of solvation, aggregate shape, and some odd temperature sensitivities,[21,22] DOSY comes into play in this study. A bevy of 2-D NMR spectroscopies can reveal structures of aggregates containing magnetically inequivalent subunits,[8e,f,23] but we had little luck with this approach on the Oppolzer enolates.

The method of continuous variations (MCV) offered us a flexible tool to ascertain the structures of enolates in solutions.[5−7] An ensemble generated from binary mixtures of constitutionally similar species of unknown aggregation number ($\mathbf{A}_n$ and $\mathbf{B}_n$, eq 2) is monitored by NMR spectroscopy as a function of mole fraction, X_A or X_B. The number and symmetries of the heteroaggregates attest to the aggregation state. Plotting the relative proportions against the measured mole fraction[24] with a parametric fit affords a Job plot confirming the assignment (*vide infra*).[7]

$$\mathbf{A}_n + \mathbf{B}_n \Rightarrow \mathbf{A}_n + \mathbf{A}_{n-1}\mathbf{B}_1 + \mathbf{A}_{n-2}\mathbf{B}_2 + \ldots + \mathbf{B}_n \quad (2)$$

The application of MCV requires carefully chosen binary mixtures to optimize spectral resolution, which becomes an issue of increasing importance as the aggregation states increase. As we show below, binary mixtures of antipodes of a single enolate—scalemic mixtures—proved especially important by reducing the resonance counts owing to symmetry. The choice of substrate is always an important issue, but it proved critical in Oppolzer enolates. Various binary pairs often provided well-resolved views of some but not all structural forms. The large number of enolates examined (Chart 2) does not reflect an unchecked urge to characterize every imaginable enolate but rather a struggle to solve some difficult problems. The data collectively lead to a self-consistent structural model assembled from a large number of combinations of substrates and solvents. As an aside, tetramer ensembles in toluene require aging at 0 °C to equilibrate the aggregates.[8,25] We suspect that the potential consequences of slow aggregate aging are underappreciated by practitioners using lithium enolates.[8a,d,e]

Chart 2. Substrates and Enolates

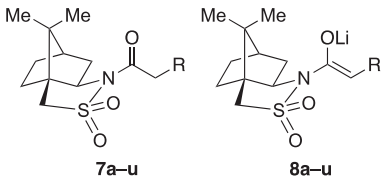

a; H	**h**; *t*-Bu	**o**; Ph
b; Me	**i**; CH_2CF_3	**p**; *p*-Cl-Ph
c; Et	**j**; $CH{=}CH_2$	**q**; *p*-MeO-Ph
d; *n*-Pr	**k**; $CH_2CH{=}CH_2$	**r**; *o*-F-Ph
e; *n*-Bu	**l**; CH_2Ph	**s**; *m*-F-Ph
f; *i*-Pr	**m**; CH_2-*m*-F-Ph	**t**; *p*-F-Ph
g; cyclohexyl (Cy)	**n**; CH_2-*p*-F-Ph	**u**; *m*-CF_3-Ph

Density functional theory (DFT) computations supported experimentally elusive details.[26−28] In what may seem intellectually backward to some, three crystal structures support the spectroscopic and computational conclusions.

RESULTS

Aggregates ebb and flow with the choice of solvent that included toluene, THF, HMPA, and combinations of the three. A standard protocol involves titrating enolate solutions in one solvent with variable concentrations of another and monitoring the appearance and disappearance of aggregates. The Oppolzer enolates were examined using ^{1}H, ^{6}Li, ^{13}C, ^{15}N, ^{19}F, and ^{31}P NMR spectroscopies; ^{6}Li, ^{13}C, and ^{19}F were the most informative. ^{15}N NMR spectroscopy using an ^{15}N-labeled substrate lacked adequate resolution within the all-important ensembles. ^{31}P NMR spectroscopy provided a few insights into lithium-HMPA contacts but generally was disappointing when compared with the successes enjoyed by Reich at low temperatures inaccessible to us.[15b] The majority of spectra are archived in the Supporting Information and not mentioned herein.

https://doi.org/10.1021/jacs.2c09341
J. Am. Chem. Soc. XXXX, XXX, XXX−XXX

There are four recurring structural types—monomers, symmetric dimers, spirocyclic dimers, and tetramers—and different forms were best observed with different enolates and ensembles. We have attempted to minimize the discomfort of the reader by using data *emblematically* to illustrate structural and stereochemical issues without attempting to adjudicate the assignments comprehensively. The presentation below is organized in an aggregate-centric format to illustrate key issues and strategies, beginning with monomers. An overview of the results presented using a more solvent-centric narrative is found in the Discussion.

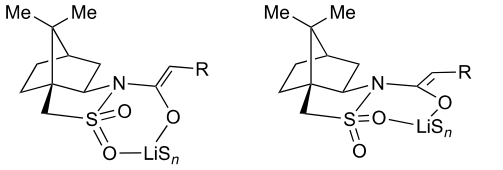

12 (*endo*)

13 (*exo*)

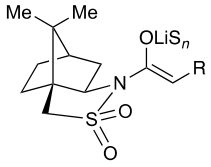

14

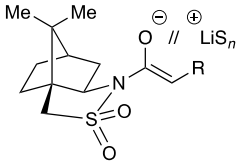

15

Monomers. The absence of detectable heteroaggregation by ^{1}H, ^{6}Li, ^{13}C, and ^{19}F NMR spectroscopies in binary mixtures of enolates is the primary evidence of a monomer. Figure 1 shows select ^{19}F NMR spectra of representative aryl

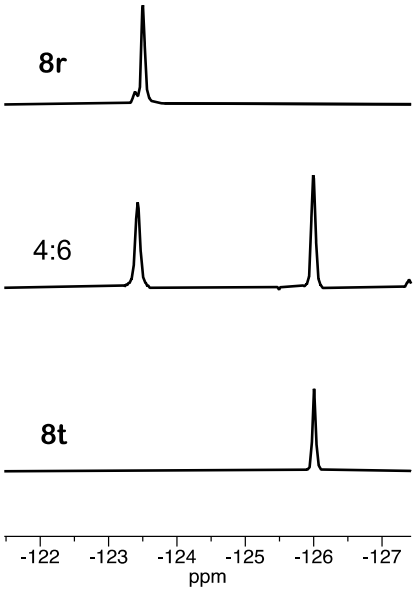

Figure 1. ^{19}F NMR spectra of 0.10 M [^{6}Li]**8r**, [^{6}Li]**8t**, and a 4:6 mixture in 0.30 M HMPA in toluene at −80 °C.

acetamide-derived enolates, a subset of Oppolzer enolates that are most prone to form monomers.[29] Possible structural variations of the monomers include **12**−**15**. The *exo* and *endo* designations refer to chelation by the sulfonyl oxygens on the *exo* and *endo* norbornyl faces, respectively. *Endo* and *exo* coordination was never observed concurrently, preventing us from distinguishing a high stereochemical preference for one from a rapid exchange of a mixture. DFT computations support 1−6 kcal/mol preferences for *endo* isomers in most aggregation states; however, there are exceptions, and both are represented in crystal structures of dimers (below). Neither unchelated monomer **14** nor ion pair **15** is detected spectroscopically,[30] but **15** proves mechanistically important. Assignment of the enolate geometries as *Z* isomers derives from putative A-strain in all carboxamide-like enolates,[31] the X-ray structures discussed below, and DFT computations. NOE studies were not definitive.

HMPA-solvated enolates are central to this study because HMPA is required for successful alkylations. Although the alkyl-substituted enolates show no evidence of HMPA-solvated monomers, additions of >1.5 equiv of HMPA to the aryl-substituted enolates show monomers emerging concurrently with dimers; monomers become the dominant form at >3.0 equiv of HMPA. They appear at characteristic chemical shifts as broad singlets, broad triplets, or well-resolved 1:2:1 triplets depending on the substrate and temperature.[32] Figure 2 shows

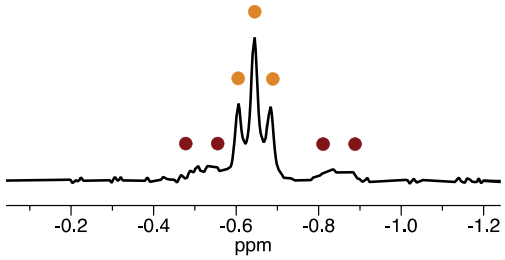

Figure 2. ^{6}Li NMR spectrum of 0.10 M [^{6}Li]**8u** in 0.30 M HMPA in toluene at −100 °C showing monomer **16** (orange) along with a bridged trisolvated dimer **24** (red, *vide infra*).

monomer **16** (R = *m*-CF_3Ph) as a 1:2:1 triplet centered at −0.64 ppm (J_{Li-P} = 3.2 Hz) flanked by two low-intensity multiplets corresponding to dimers (*vide infra*). ^{31}P NMR spectroscopy shows two ^{31}P resonances (1:1) broadened by unresolved ^{6}Li coupling, which logically correspond to the *endo*- and *exo*-disposed HMPA ligands of **16**. DFT computations support **16** over the *exo* chelate by 4.9 kcal/mol.

The *bis*-HMPA solvation confirms that the chelate remains intact rather than forming **14** or **15** based on extensive studies of HMPA-solvated lithium salts by Reich.[15b] DOSY showed that monomer **16** has a lower relative molecular weight than trisolvated dimers (discussed below), confirming that the triplet stems from the relatively small monomer **16** rather than from a relatively large tetrasolvated dimer of general structure $(ROLi)_2(HMPA)_4$.

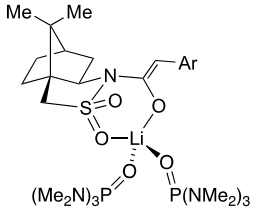

16 (*endo*)

Dimers. We are presented not only with the complexity of *endo* versus *exo* chelation but also by what we colloquially refer to as symmetric dimers (**17** and **18**) and spirocyclic dimers (**19** and **20**). A crystal structure of enolate **8c** reveals dimer **22** (Figure 3), which corresponds to homochiral dimer **17** (R = ethyl) showing coordination to the *endo* sulfonyl oxygen with

https://doi.org/10.1021/jacs.2c09341
J. Am. Chem. Soc. XXXX, XXX, XXX−XXX

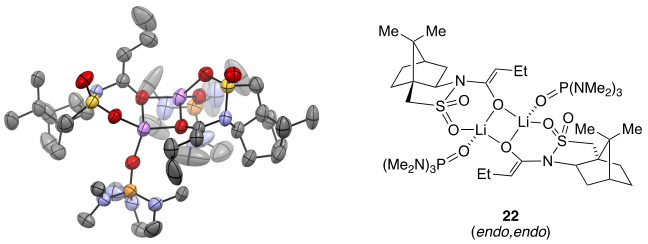

Figure 3. X-ray crystal structure of *bis*-HMPA solvated enolate **8c** corresponding to homochiral dimer **22** showing double *endo* chelation with one HMPA on each lithium *syn* to each other.

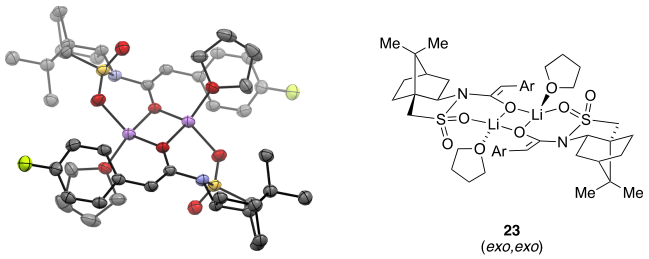

Figure 4. X-ray crystal structure of *bis*-THF solvated enolate **8t** corresponding to *heterochiral* dimer **23** (Ar = *p*-fluorophenyl) showing double *exo* chelation with one THF on each lithium *anti* to each other.

one HMPA on each lithium *syn* to each other. A 7:3 scalemic mixture of aryl-substituted enolate **8t** (Figure 4) affords dimer **23**, which corresponds to *heterochiral* dimer **21** (R = *p*-fluorophenyl) showing chelation by the *exo* sulfonyl oxygen with one THF on each lithium *anti* to each other.

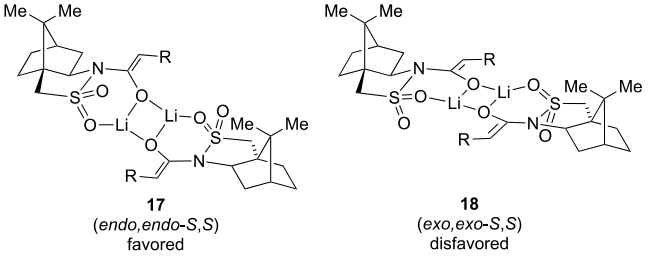

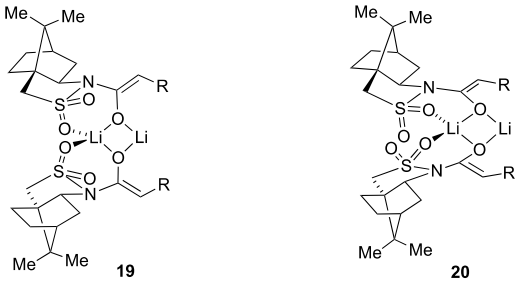

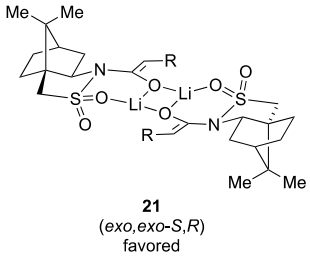

Symmetric dimers such as **17** or **18** have magnetically equivalent subunits and would display a single ^{6}Li resonance. The spirocyclic dimers **19** and **20** display two well-resolved ^{6}Li nuclei while displaying magnetically equivalent subunits. Select spectra of enolates **8b** and **8g** (Figure 5) and the affiliated Job plot (Figure 6) confirm the dimer assignment. An alternative view using scalemic mixtures of **8t** affording magnetically identical $\mathbf{A}_2$ and $\mathbf{B}_2$ homodimers provides the Job plot in Figure 7.[6] The nonstatistical preference for heterodimerization in Figure 7—the two curves should meet at 0.50 relative intensity and X_S = 0.50 in a statistical sample—is supported by DFT suggesting a 2.2 kcal/mol preference.

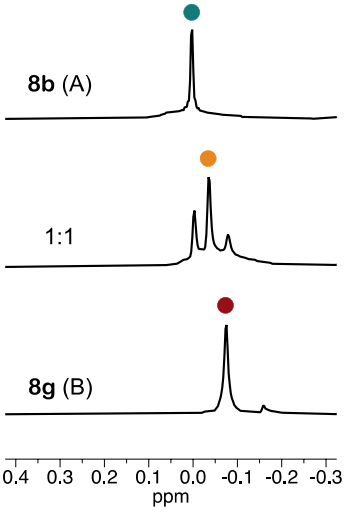

Figure 5. ^{6}Li NMR spectra of 0.10 M mixtures of [^{6}Li]**8b** ($\mathbf{A}_2$, blue) and [^{6}Li]**8g** ($\mathbf{B}_2$, red) in neat THF at −80 °C. One new resonance appears for the mixed aggregate ($\mathbf{A}_1\mathbf{B}_1$, orange).

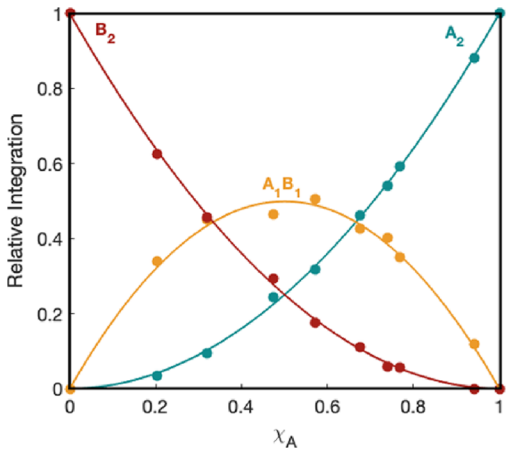

Figure 6. Job plot showing relative integrations of homodimers of [^{6}Li]**8b** ($\mathbf{A}_2$, blue) and [^{6}Li]**8g** ($\mathbf{B}_2$, red) and the heterodimer ($\mathbf{A}_1\mathbf{B}_1$, orange) plotted against the measured mole fraction[24] of [^{6}Li]**8b** (X_A) for 0.10 M mixtures of lithium enolates [^{6}Li]**8b** and [^{6}Li]**8g** in neat THF at −80 °C monitored by ^{6}Li NMR spectroscopy (Figure 5). The curves result from a parametric fit to a dimer model.

Conjugation-stabilized aryl acetamide-derived enolates in toluene afford homoaggregated spirocyclic dimers (**19** or **20**) manifesting magnetically equivalent enolate subunits and two inequivalent lithium nuclei to the exclusion of higher aggregates. Although the ^{6}Li resonances within dimer

https://doi.org/10.1021/jacs.2c09341
J. Am. Chem. Soc. XXXX, XXX, XXX−XXX

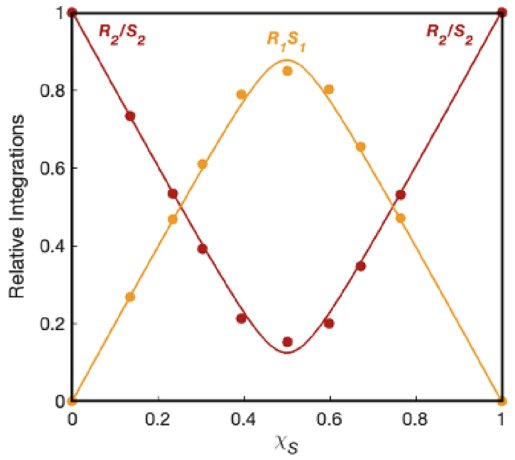

Figure 7. Job plot showing relative integrations of the two magnetically equivalent homochiral homodimers of [^{6}Li]**8t** ($\boldsymbol{R_2/S_2}$, red) and a heterochiral mixed dimer ($\boldsymbol{R_1S_1}$, orange) plotted against the measured mole fraction[24] of [^{6}Li](S)**8t** (X_S) for scalemic 0.10 M mixtures of [^{6}Li]**8t** in 10 M THF/toluene at −80 °C monitored by ^{19}F NMR spectroscopy. The curves result from a parametric fit to a dimer model.

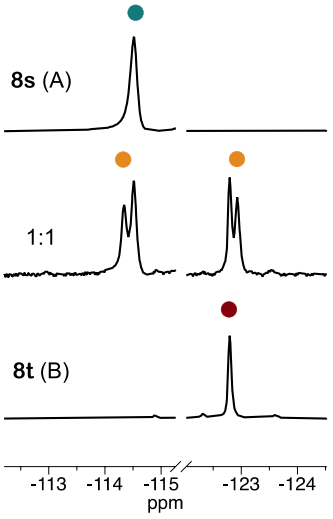

Figure 8. ^{19}F NMR spectra of mixtures of [^{6}Li]**8s** ($\mathbf{A_2}$, blue) and [^{6}Li]**8t** ($\mathbf{B_2}$, red) in toluene at −80 °C. Two new resonances appear for the mixed aggregate ($\mathbf{A_1B_1}$, orange).

ensembles were poorly resolved, ^{19}F NMR spectroscopy (Figure 8) provided the resolution for a clean dimer-based Job plot (Supporting Information).[33]

Incremental additions of HMPA to enolates in THF or toluene showed a recurring theme in which a single ^{6}Li resonance of variable intensity corresponding to monomer **16** (monomer type **12**) as discussed above was flanked by two equal-intensity ^{6}Li resonances. Resolution of the ^{6}Li-^{31}P couplings was substrate-dependent; enolate **8o** provided a particularly clear view (Figure 9). The two doublet-of-doublets ($J_{Li\text{-}P}$ = 3.2 and 1.1 Hz) first noted in Figure 2 correspond to a bridged dimer with a partial structure **24**. Monomer **16** is favored at elevated HMPA concentrations and low enolate concentrations, consistent with higher per-lithium solvation and lower aggregation than **24**. The small coupling in **24** is characteristic of bridged (μ_2) HMPA ligands.[15b]

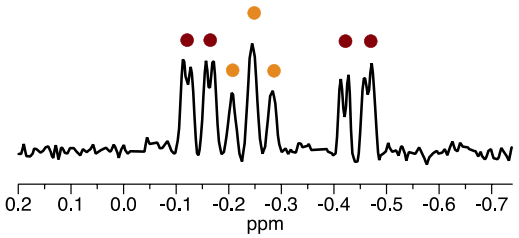

Figure 9. ^{6}Li NMR spectrum of 0.10 M [^{6}Li]**8o** in 0.30 M HMPA in toluene at −100 °C showing bridged trisolvated dimer **24** (red) and monomer **16** (orange).

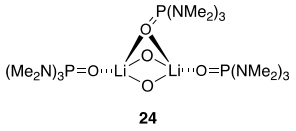

24

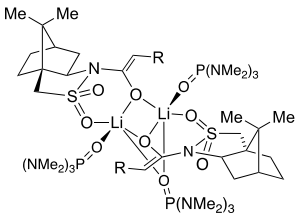

25
(*endo,exo*)

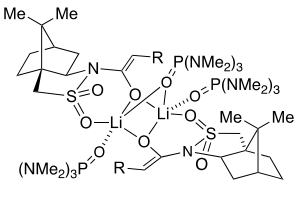

26
(*endo,exo*)

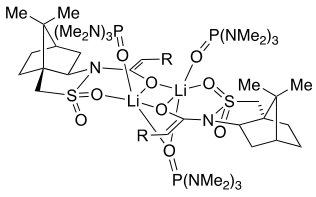

27
(*exo,exo*)

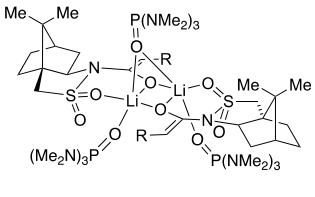

28
(*exo,exo*)

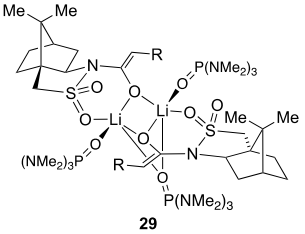

29
(*endo,endo*)

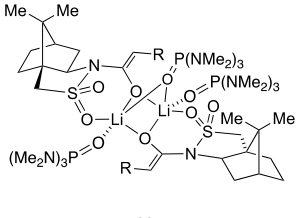

30
(*endo,endo*)

The partial structure **24** with requisite proximal (synfacial) HMPA ligands is consistent with the HMPA ligands in the crystallographically characterized disolvated dimer (Figure 3). Moreover, *two* doublet-of-doublets (1:1) suggest an asymmetry that would arise from magnetically inequivalent subunits. This lack of symmetry seems to demand either a single *endo*–*exo* pairing such as **25** or **26** or a 1:1 mixture of two symmetric dimers out of four possible isomers, **27**–**30**. The invariant 1:1 proportions of the two double-of-doublets in numerous examples seem too coincidental, prompting us to lean firmly toward **25** or **26**. Computations of the six isomers showed **25** to be strongly preferred relative to **30**, whereas stable minima with intact core structures could not be located for dimers **26**–**29**.

Tetramers. Tetramers of general structure **31** with D_{2d}-symmetric cores manifesting a single ^{6}Li resonance and magnetically equivalent subunits had been observed for lithiated Evans enolates (**5**).[8d] Tetramers with S_4-symmetric

https://doi.org/10.1021/jacs.2c09341
J. Am. Chem. Soc. XXXX, XXX, XXX−XXX

cores (**32**) manifesting two ^{6}Li resonances (1:1) and two magnetically inequivalent subunits were observed for chiral amino alkoxides.[34,35] Both forms are well represented crystallographically for tetrameric chelated lithium salts. Alkyl-substituted Oppolzer enolates (**8a−n**) in toluene uniformly display the spectral properties anticipated for **32**. Computations using propionate enolate **8b** reveal an 11 kcal/mol preference for **32** over **31**.

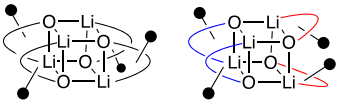

31 (D_{2d} core) **32** (S_4 core) observed

Confirming the tetramer assignment by MCV was particularly challenging because of isomerism within the 3:1, 2:2, and 1:3 heteroaggregates (Chart 3). A complete ensemble

Chart 3. Ensemble of Homo- and Heteroaggregated Tetramers and Affiliated Resonance Counts

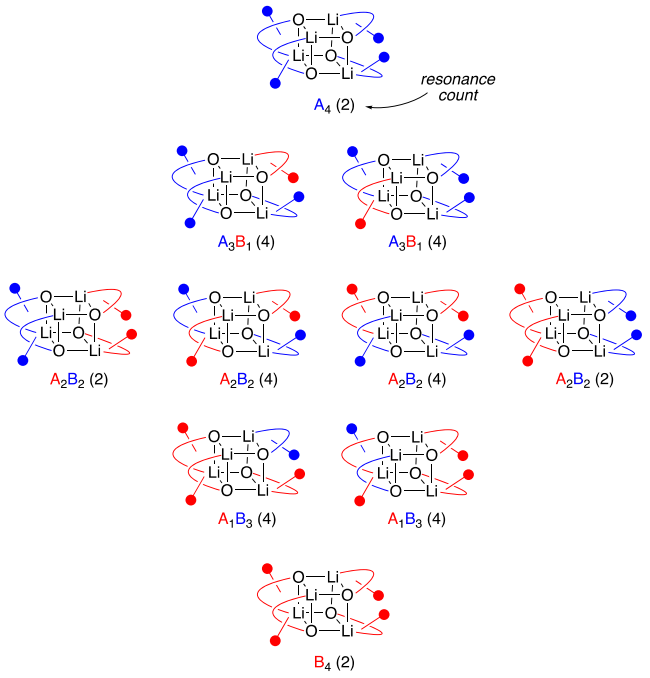

of S_4-type tetramers in the limit consists of 10 discrete isomers manifesting 32 magnetically distinct subunits. Although relief from steric congestion might drive stereocontrol and preclude some isomers, success was not guaranteed. In previous examples, we could monitor aggregate proportions at elevated temperatures wherein each stoichiometry in the $\mathbf{A}_n-\mathbf{B}_n$ ensemble appears as a single ^{6}Li resonance owing to *intra-aggregate* ^{6}Li-^{6}Li exchange.[5,34] Unfortunately, Oppolzer enolates in toluene decompose above 0 °C, temperatures well below those needed to observe intra-aggregate coalescence.

The most tractable result emerged from mixtures of **8f** and **8l**, affording 18 identifiable ^{6}Li resonances in total. Monitoring the intensities against mole fraction (Figure 10), paying particular attention to mass action effects to discern the different stoichiometries, afforded tentative assignments to the various aggregate stoichiometries and the Job plot in Figure 11. Although this confirms high (tetramer-like) aggregation

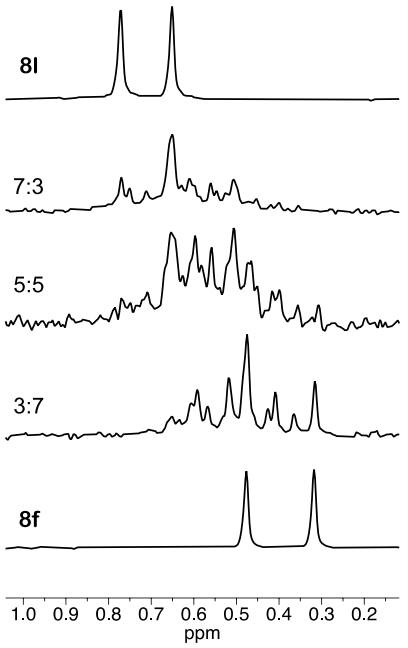

Figure 10. Select ^{6}Li NMR spectra of mixtures of [^{6}Li]**8l** ($\mathbf{A}_4$) and [^{6}Li]**8f** ($\mathbf{B}_4$) in toluene at −80 °C. The sealed NMR tubes were aged at 0 °C for 10 min. The total molar ratio (**8l**/**8f**) of the two enolates is superimposed to the left of each spectrum. Several new overlapping resonances appear for the mixed aggregates ($\mathbf{A}_3\mathbf{B}_1$, $\mathbf{A}_2\mathbf{B}_2$, $\mathbf{A}_1\mathbf{B}_3$) consistent with a tetramer model.

behavior, the reliance on precise attributions seems fanciful. Fortunately, a much better solution arose.

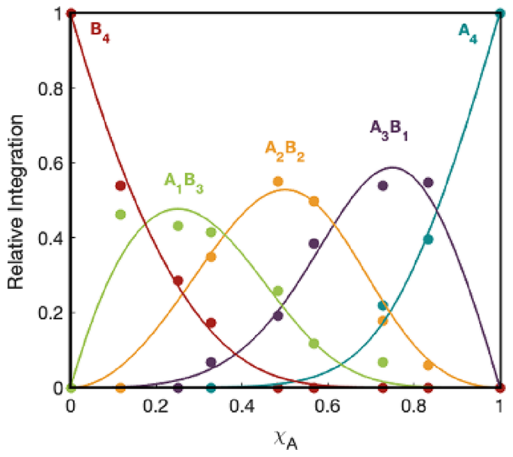

Figure 11. Job plot showing relative ^{6}Li integrations (Figure 10) of the two homoaggregates of [^{6}Li]**8l** ($\mathbf{A}_4$, blue) and [^{6}Li]**8f** ($\mathbf{B}_4$, red), 3:1 mixed tetramer $\mathbf{A}_3\mathbf{B}_1$ (violet), 2:2 mixed tetramer $\mathbf{A}_2\mathbf{B}_2$ (orange), and 1:3 mixed tetramer $\mathbf{A}_1\mathbf{B}_3$ (green) against the measured[24] mole fraction of [^{6}Li]**8l** (X_A) for 0.10 M mixtures of lithium enolates [^{6}Li]**8l** and [^{6}Li]**8f** in neat toluene at −80 °C. The curves result from a parametric fit to a tetramer model.

Binary mixtures of two enantiomers reduce the number of possible structures (Chart 4) *and* the number of resonances owing to enantiomeric $\boldsymbol{R}_4/\boldsymbol{S}_4$, $\boldsymbol{R}_3\boldsymbol{S}_1/\boldsymbol{R}_1\boldsymbol{S}_3$, and $\boldsymbol{R}_2\boldsymbol{S}_2$ aggregate pairs and generally higher symmetries within several heterotetramers. The theoretical upper limit drops to 6 discrete aggregates displaying 12 ^{6}Li resonances. We suspected that stereocontrolled aggregation might further reduce the

https://doi.org/10.1021/jacs.2c09341
J. Am. Chem. Soc. XXXX, XXX, XXX−XXX

Chart 4. Ensemble of Homo- and Heteroaggregated Tetramers from Scalemic Mixtures and Affiliated Resonance Counts

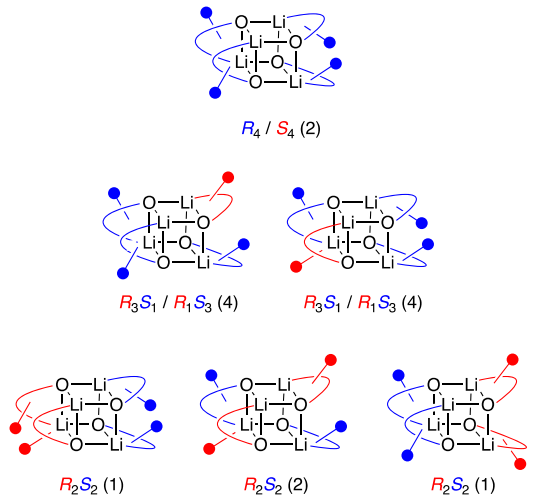

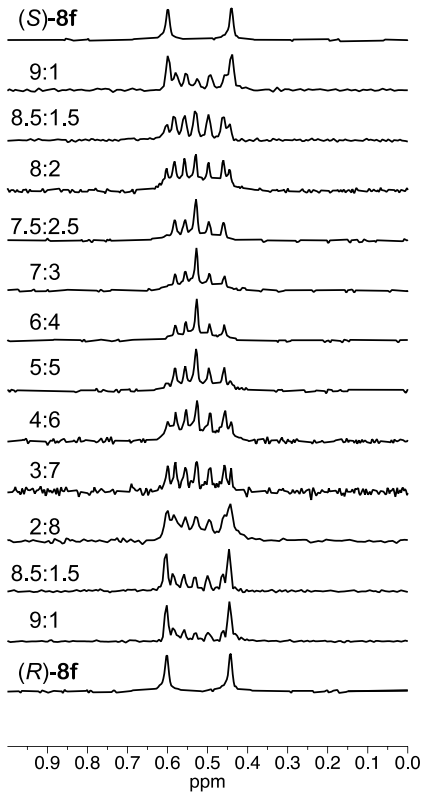

Figure 12. ^{6}Li NMR spectra of mixtures of the two antipodes of [^{6}Li]**8f** in toluene at −80 °C and aged at 0 °C for 10 min.[25] The *intended* (not measured) molar ratio (*S*:*R*)[24] of the two enolates is to the left of each spectrum. Five new resonances appear for the mixed aggregates ($\boldsymbol{R_3S_1}$, $\boldsymbol{R_2S_2}$, $\boldsymbol{R_1S_3}$) consistent with a tetramer model.

number of resonances. In the optimistic event of *total* stereocontrol producing a single stereoisomeric heteroaggregate for each stoichiometry, the theoretical aggregate count drops to three and the resonance count drops to seven.

We got lucky. Three enantiomeric pairings each afforded the optimal stereocontrol manifesting only *seven* resonances, affording successful MCV analyses; scalemic mixtures of the isopropyl substituted enolate **8f** gave the most visually pleasing

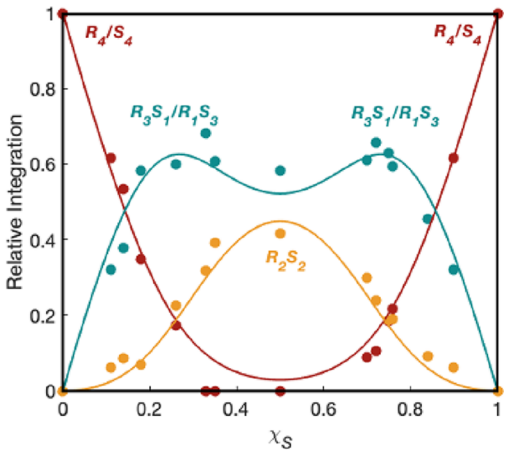

Figure 13. Job plot showing relative integrations plotted against the measured[24] mole fraction of the *S* antipode (X_S) in 0.20 M scalemic mixtures of lithium enolate [^{6}Li]**8f** in neat toluene at −80 °C monitored by ^{6}Li NMR spectroscopy (Figure 12). The curves showing mirror image homotetramers ($\boldsymbol{R_4}$/$\boldsymbol{S_4}$, red), mirror image 3:1 heterotetramers ($\boldsymbol{R_1S_3}$/$\boldsymbol{R_3S_1}$, blue), and a single 2:2 heterotetramer ($\boldsymbol{R_2S_2}$, orange) result from a parametric fit to a tetramer model.

spectra (Figure 12) and Job plot (Figure 13). The 2:2 stoichiometry, for example, displays a single resonance out of a possible four. We are fully confident in the tetramer assignment and find the stereochemical complexity of aggregation quite satisfying (in retrospect).

We examined the heterochiral ensemble using DFT. The 3:1 and 2:2 mixed tetramers showed 6.0 and 4.0 kcal/mol preferences, respectively, for single isomers. An observed small nonstatistical preference for forming the 3:1 and 2:2 heterotetramers observable in Figure 13—the blue and orange curves should contact at X_S = 0.5—is overestimated computationally (2.0 and 1.7 kcal/mol, respectively.)

Influence of Excess LDA. A standard protocol of probing for lithium enolate-LDA mixed aggregates by using excess [^{6}Li,^{15}N]LDA revealed dianion crudely depicted as **33** instead (eq 3).[36] Three distinct ^{6}Li resonances (2:1:1) showed no ^{6}Li-^{15}N coupling. A crystal structure showed a complex aggregate composed of four subunits of dianion **33** with symmetry consistent with the ^{6}Li spectral data (Figure 14).

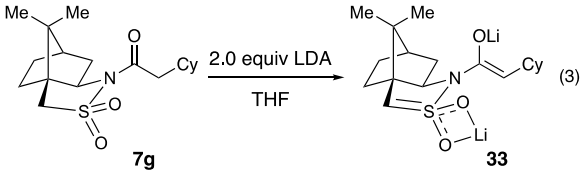

There are no C−Li contacts. The structure of the dianion is of limited pedagogical value except to reveal the origins of byproducts reported in the synthetic organic literature discussed below.[37] The $Li_8O_{12}X_4$ core structure does not appear in the Cambridge Database.

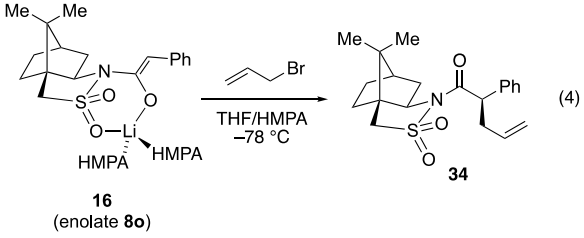

https://doi.org/10.1021/jacs.2c09341
J. Am. Chem. Soc. XXXX, XXX, XXX−XXX

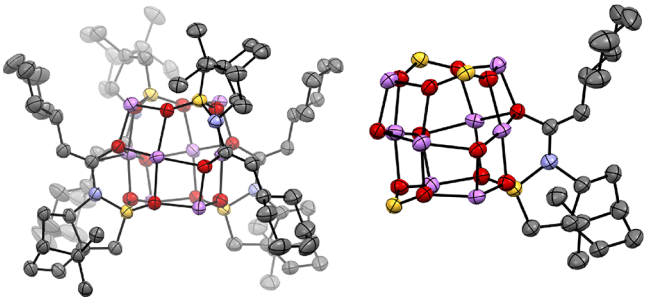

Figure 14. Partial X-ray crystal structure of *octalithiated* tetramer with D_2 symmetry consisting of four units of dianion **33** (left) and partial structure (right). Six coordinated THF molecules have been omitted for clarity.

Kinetics of Alkylation.[38] The mechanism of alkylation was studied using enolate **8o** and allyl bromide (eq 4). The enolate generated in situ using recrystallized LDA[39] exists as *bis*-HMPA-solvated monomer **16** (R = Ph) over all concentrations of HMPA (0.075−0.90 M), THF (0.50−11.0 M), and allyl bromide (≤0.825 M).[40] Alkylation rates were monitored by in situ IR spectroscopy[41] following the loss of enolate **8o** (1616 cm^{-1}) and formation of product **34** (1704 cm^{-1}). Figure 15 illustrates an emblematic decay. Alkylations

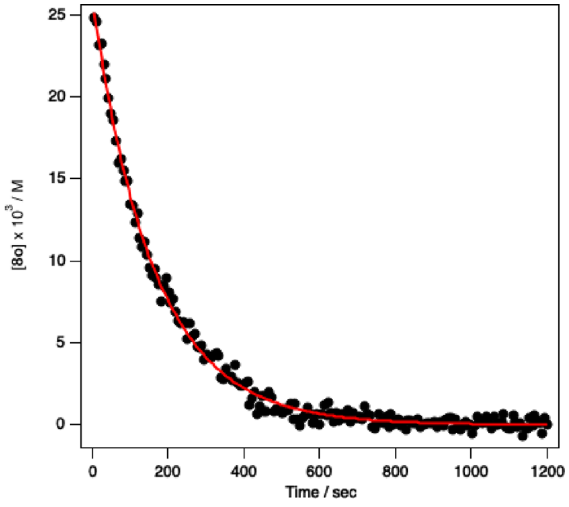

Figure 15. Alkylation of **8o** (0.025 M; 1616 cm^{-1}) with 0.275 M allyl bromide in 9.00 M THF/toluene at −78 °C to form **34** (1704 cm^{-1}). The red curve depicts an unweighted least-squares fit to eq 5 such that $n = 1.01 \pm 0.02$, $k_{obsd} = 0.0064 \pm 0.0005$, and $[substrate]_0 = 0.0261 \pm 0.0002$.

under more synthetically relevant conditions (0.10 M enolate and 3.0 equiv of allyl bromide) displayed no unusual curvatures that would be emblematic of intervening consequential autocatalysis or autoinhibition.[38d]

With enolate as the limiting reagent and boxed in by technical limitations owing to substrate solubilities, we turned to the nonlinear variant of the van't Hoff differential method (eq 5)[42] to determine the enolate order, *n*, by best fit. The curve in Figure 15 stems from such a fit. Although orders determined by this method routinely afford considerable variation from run to run, replication solves that problem. An enolate order of 1.2 ± 0.2 was obtained from the 132 independent decays used to obtain values for k_{obsd}. The first order in excess allyl bromide was confirmed by a two-point control experiment showing a direct relationship of k_{obsd} to concentration.

$$[\text{enolate}] = \{[\text{enolate}]_0^{(1-n)} - (n-1)k_{obsd}t\}^{1/(1-n)} \quad (5)$$

A plot of k_{obsd} against [HMPA] concentration reveals a second-order dependence (Figure 16) that implicates an

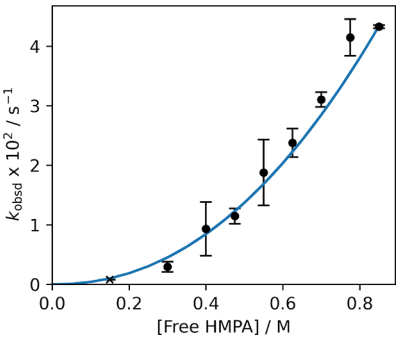

Figure 16. Plot of k_{obsd} against [HMPA] for the alkylation of enolate **8o** (0.025 M) with 0.275 M allyl bromide in 9.0 M THF/toluene at −78 °C. The asterisk (*) to the far left is outside pseudo-first-order conditions and was not included in the fit. The blue curve depicts an error-weighted least-squares fit to $f(x) = ax^b$ such that $a = 0.062 \pm 0.001$ and $b = 2.2 \pm 0.1$.

intermediate ion pair or free ion with a $^+Li(HMPA)_4$ counterion commonly observed spectroscopically.[15b] The first-order rather than half-order enolate dependence implicates ion pair **35** with correlated ions rather than fully formed free ions, which would manifest a half-order dependence.[43]

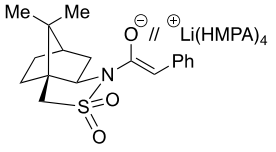

35

A plot of k_{obsd} against THF concentration revealed a second-order THF dependence (Figure 17, blue curve). Superficially, this implicates a $^+Li(HMPA)_4(THF)_2$ cation. However, using

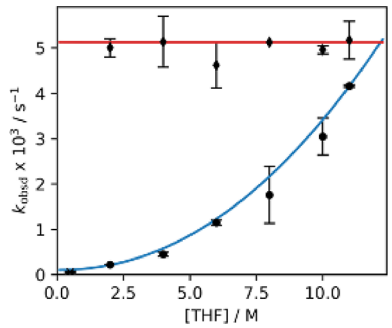

Figure 17. Plot of k_{obsd} against THF concentration for alkylation of 0.025 M **8o** with allyl bromide (0.275 M) in 0.275 M *free* HMPA concentration[46] at −78 °C in toluene (●) or 2,5-Me_2THF (◆) cosolvent. The asterisk (*) to the far left is not under pseudo-first-order conditions and was not included in the fit. The blue curve depicts an error-weighted least-squares fit to the function $f(x) = y_0 + ax^b$ such that $y_0 = 1.0 \times 10^{-4} \pm 0.1 \times 10^{-4}$, $a = 2.5 \times 10^{-5} \pm 0.4 \times 10^{-5}$, and $b = 2.1 \pm 0.1$. The red curve depicts an error-weighted least-squares fit to the function $f(x) = y_0 + ax$ such that $y_0 = 4.9 \times 10^{-3} \pm 0.2 \times 10^{-3}$ and $a = 1.1 \times 10^{-5} \pm 2.9 \times 10^{-5}$.

https://doi.org/10.1021/jacs.2c09341
J. Am. Chem. Soc. XXXX, XXX, XXX−XXX

toluene as the cosolvent proved to be a fateful choice. Suspecting from previous studies that secondary-shell (medium) effects could be intervening, we carried out a standard control experiment in which 2,5-Me_2THF was used as a sterically encumbered (noncoordinating) cosolvent with a dielectric constant nearly equal to that of THF.[44] The resulting *zeroth*-order THF dependence is shown in Figure 17 (red curve). Thus, the second-order THF dependence is entirely attributable to sterically insensitive medium effects, which seemed extraordinary based on numerous previous studies in which most but not all reveal trivial cosolvent dependencies. Having observed strange effects of toluene on several occasions,[45] we monitored the initial rate against toluene concentration using cyclopentane as cosolvent at fixed HMPA and THF concentrations and obtained an inverse-first-order dependence (Figure 18). These sterically insensitive (secondary-shell) effects are considered further in the discussion.

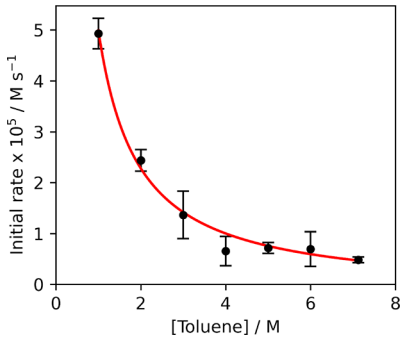

Figure 18. Plot of rate constants determined from initial rate measurements against toluene concentration for the alkylation of 0.025 M **8o** at −78 °C with 0.275 M allyl bromide in 0.275 M *free* HMPA in 2.0 M THF using cyclopentane cosolvent. The curve depicts an error-weighted least-squares fit to the function $f(x) = y_0 + ax^b$ such that $y_0 = -1.4 \times 10^{-6} \pm 0.3 \times 10^{-6}$, $a = 5.1 \times 10^{-5} \pm 0.3 \times 10^{-5}$, and $b = -1.1 \pm 0.2$.

DISCUSSION

We have described one of those investigations that might have given us pause had we anticipated the challenges. The structural studies provided inordinate complexity, whereas the rate studies offered unexpected results. We begin by summarizing the structural studies described above and archived in the Supporting Information by taking a solvent-centric look at aggregation, underscoring the general trends.

Solvent- and Substituent-Dependent Aggregation. Scheme 1 depicts the structural changes of Oppolzer enolates as a function of solvent, taking liberties to make the story tractable. The loops represent the sultam chelates, whereas the sticks and spheres reflect different faces with implicitly different steric demands. The loose term "solvent power" connotes the progression through a combination of increasing solvent donicity[47] (Lewis basicity) and increasing donor solvent concentration, which tend to work in concert.

Oppolzer enolates in toluene exist as two structural types depending on the enolate substituent. The sterically unhindered alkyl-substituted enolates afford tetramers of type **32** with S_4-symmetric cores analogous to lithium amino alkoxides in solutions[34] rather than drum-like structures with D_{2d}-symmetric cores (**31**) formed by Evans enolates (**5**, Chart 1).[8d,48] This is supported by DFT computations showing an 11

Scheme 1. Solvent-Dependent Aggregates of Oppolzer Enolates

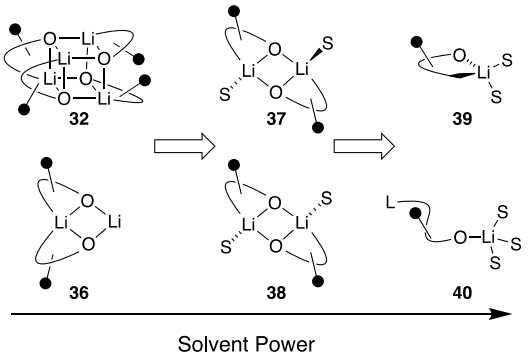

kcal/mol preference isomer **32**. Primary-shell solvation (ligation) by toluene is implicated only in the spirocyclic dimer structures (see below), but toluene strikingly influences reactivity (*vide infra.*)

Ironically, our first efforts to explore tetramers computationally using phenylacetate-derived enolate **8o** as a model completely failed to afford stable minima with the cubic core intact. We subsequently discovered that the relatively large phenyl groups[49] preclude the formation of tetramers, affording the spirocyclic dimers (**36**) instead. Enolates **8f** and **8g** bearing large alkyl substituents form tetramer **32** along with low levels of spirocycle **36**. DFT suggests a 2.0 kcal/mol exothermic solvation of the terminal lithium of **36** by toluene (Figure 19).

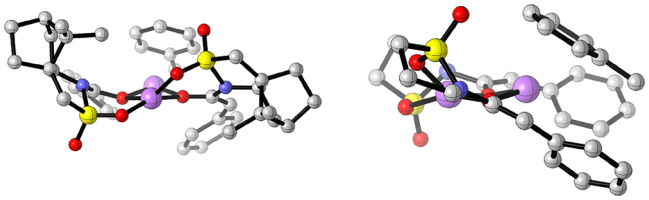

Figure 19. DFT-computed structure of phenyl-substituted enolate **8o** displaying a type-**36** core structure. The partial structure illustrates the disposition of the ligated toluene measurably out of the Li_2O_2 plane.

The partial structure in Figure 19 shows an interesting gearing of the three phenyl moieties. Although this should render the two subunits magnetically inequivalent, high fluxionality would be expected to obscure the broken symmetry.

We routinely study solvation by titrating hydrocarbon solutions of organolithiums with donor solvent to observe structural changes during the transition from the large aggregates to more highly solvated lower aggregates.[7] This strategy provided complex and largely useless spectra at low THF concentrations en route to the tractable dimers emerging at elevated (typically >3.0 M) THF concentrations. Both alkyl- and aryl-substituted enolates afford symmetric solvated dimers **37** or **38**. THF solvates with *anti*-oriented THF ligands (**37**) are assigned based on DFT computations and analogy to a crystal structure in Figure 4. These THF-solvated dimers proved well-suited for MCV-based characterizations and would have been excellent candidates for mechanistic studies if not for their failure to alkylate below the temperatures of enolate decomposition.

Incrementally adding HMPA to toluene and various THF−toluene mixtures revealed several resonances that were candidates for the *bis*-HMPA-solvated dimers (see **37** or **38**),

https://doi.org/10.1021/jacs.2c09341
J. Am. Chem. Soc. XXXX, XXX, XXX−XXX

but their concentrations remained low, and definitive assignments were elusive. The dominant HMPA-solvate is akin to the type-**38** dimer observed crystallographically (Figure 3) but with an additional bridging (μ_2) HMPA. This trisolvated dimer with a core structure illustrated by **24** invariably coexists with disolvated monomer of type **39**. Of six possible isomeric trisolvates (**25**–**30**), broken symmetry observed spectroscopically in conjunction with DFT computations pointed to a single isomer **25** with a mix of *endo* and *exo* chelation (Figure 20). Of the five other isomers, only **30** afforded a stable minimum with intact core structure, and it is considerably higher energy.

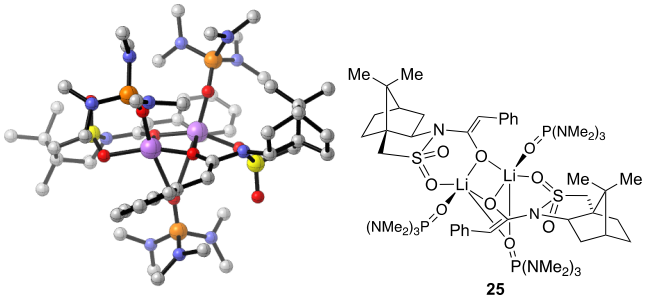

Figure 20. DFT-computed structure of *tris*-HMPA-solvated dimer **25**.

A monomer of type **39** (drawn in more detail as **16** in eq 4) containing two magnetically inequivalent HMPA ligands forms to the exclusion of **40** that would be at least trisolvated according to Reich's extensive studies of HMPA solvation.[15b] Most importantly, type-**39** monomers form over a wide range of conditions for aryl-substituted enolates, establishing structural foundations for rate studies. Before addressing the alkylation mechanism and its role in dictating stereoselective alkylation, however, there are a few structural details to consider.

Stereochemistry of Aggregation. Something so simple as whether the sultam chelate exploits the *exo* or *endo* sulfonyl oxygen remains unresolved spectroscopically; the *endo* form is preferred computationally in most environments, whereas both are represented crystallographically. Stereochemical issues that emerged when using MCV to determine aggregation state are primarily academic but are interesting nonetheless. One can argue that understanding stereocontrolled aggregation may reveal how to exploit homo- and heteroaggregate structures to impose stereocontrol on tetramer-based transformations.[14,50] Probably the most spectacular example of this was achieved by Merck Process in their efavirenz synthesis.[51]

Characterizing S_4-type tetramers using MCV relies on generating ensembles of two structurally distinct enolates with up to 32 magnetically inequivalent subunits (Chart 3). By contrast, pairing *enantiomers*—generating analogous R_mS_n ensembles from scalemic mixtures—reduces the number of possible magnetically equivalent subunits to 12 (Chart 4). In the limit that steric biases impart total diastereoselectivity, the resulting heterochiral ensembles could reduce to as few as three distinct tetramers manifesting only seven magnetically distinct subunits. That is *precisely* what happened as illustrated by the clean ensembles and convincing Job plots (Figures 12 and 13).

Dianion. Synthetic chemists have reported byproducts of type **41** in which LDA appeared to metalate proximate to the sulfonyl group.[37] Our quest for evidence of LDA-enolate mixed aggregates instead afforded **33** as a spectroscopically and crystallographically characterized octalithiated tetramer (Figure 14). The dianion did not form mixed aggregates with LDA, which contrasts with dianion **6** corresponding to Myers enolates (Chart 1).[8e]

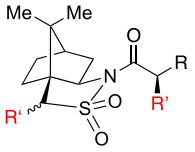

Despite square planar lithiums and no C–Li contacts, there is nothing particularly notable about the structure. It does, however, prompt a few comments and some ideas worth exploring. Decades ago, we rediscovered[52] the high tendency of sulfones to stabilize dianions of general structure $ArSO_2CM_2R$ (M = Li, Na, or K)[53,54] and even $ArSO_2CLi_3$.[55] In short, sulfones are remarkably effective at stabilizing anions. Synthetic organic and inorganic chemists have largely overlooked these potentially interesting synthons. We also suspect that there is a general notion within the community that dianions are destabilized by charge repulsion. To understand the flaw in this logic, compare an aggregated alkoxide to a dilithiated dialkoxide (**42** and **43**): it is altogether unclear why simply adding the bridge would be destabilizing. Moreover, given that highly reactive organolithiums routinely aggregate, invoking charge repulsion is linguistically and thermochemically suspect.

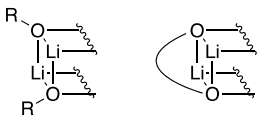

Mechanism of Alkylation and Odd Solvent Effects. Aryl-substituted enolates forming *bis*-HMPA-solvated monomers of type **16** (**39** in Scheme 1) persist over a wide range of conditions, rendering them well-suited for rate studies. A second-order HMPA dependence and first-order enolate dependence are fully consistent with a mechanism proceeding through a transition structure based on solvent-separated ion-pair **35**. The obvious loss of the chelate stands out, but before discussing the origins of stereocontrol, we must draw attention to some unusual solvent effects.

A second-order THF dependence initially suggested a hexasolvated mixed cation, $^{+}Li(HMPA)_4(THF)_2$, but was traced to *exclusively* secondary-shell (medium) effects. A superposition of an *inverse*-first-order toluene dependence and a *first*-order THF dependence was acting antagonistically: toluene stabilizes the reactant, and THF stabilizes the transition structure (Figure 21). Using 2,5-Me_2THF instead of toluene as cosolvent eliminates both effects, causing the apparent second-order THF dependence to disappear altogether.

We begin with the seemingly straightforward stabilization of the transition state by THF. Having ascertained a vast number of rate laws, we have found that medium effects in THF/hexane mixtures range from small to undetectable in most instances.[38c] In short, the medium effects in both the ground state and transition state cancel. The $^{+}Li(HMPA)_4$ gegenion, however, would logically be stabilized by secondary-shell (possibly ordered) dipoles.[15b,55] In analogy to the Oppolzer enolate alkylations, an ionization-based alkylation of Ph_2NLi in

https://doi.org/10.1021/jacs.2c09341
J. Am. Chem. Soc. XXXX, XXX, XXX–XXX

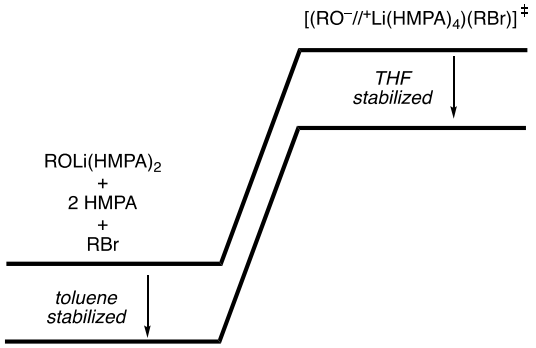

Figure 21. Medium effects on the ground and transition states.

THF[56] revealed exceedingly high THF orders that were traced to the superposition of primary- and secondary-shell influences.

Stabilization of the reactants by toluene is more nuanced but also supported by other studies. Evidence of primary-shell lithium ion coordination by aromatic hydrocarbons is well documented.[7] Although it is difficult to imagine a consequential stabilization of monomer **16**, we have observed strange effects of aromatic hydrocarbons on both observable organolithium equilibria as well as on reaction rates even in the presence of far superior donor solvents.[38d] The closest analogy to the Oppolzer enolates is found in LDA-mediated enolization of esters in THF-HMPA, also displaying a second-order HMPA dependence owing to an ion-paired intermediate.[45d] Changing the "inert" cosolvent from *pentane to cyclopentane* to help solubilize the HMPA reduced the observed rates without reducing the HMPA reaction order. We surmised that the cyclopentane-based stabilization of HMPA imparting higher solubility was the same stabilization retarding the reaction. Thus, *the enolization of esters and the alkylation of Oppolzer enolates are retarded by solvent−solvent interactions.* The notion that dissolving reactants *necessarily* has a retarding influence on reactivity is self-evident in retrospect but easily overlooked. That such rate effects are observed in the presence of notoriously more polar solvents and are attributable to solvent−solvent rather than solvent−lithium interactions is sobering. Thus, it is precarious to consider toluene an "inert" cosolvent. It is to be respected and, if necessary, avoided in detailed rate studies. We have fallen into this trap several times.[45,57,58]

Origins of the Stereoselectivity. We now must unbury the lede and ponder the origins of the highly stereocontrolled alkylations. The ion-pair-based alkylation ensures that there is no role of the chelate despite its central importance to every mechanistic model reported to date with one exception.[59] The solvent-separated ion pair even renders the lithium cation largely irrelevant.

This is where the story gets interesting. The computed structure of the cation-free enolate, **44**, shows a 131° S−N−C−O dihedral angle, which operationally reverses the faces of the enolate exposed to the steric influence of the *gem*-dimethyl groups when compared with chelated forms. DFT computations show a 3.9 kcal/mol preference for **44** over the rotamer with the enolate oxygen *syn* to sulfone. The preferred alkylation of **44** requires approach of the electrophile *syn* to the protruding camphor methyl group. Indeed, DFT computations show a 2.6 kcal/mol preference for *syn* (*exo*) approach via transition structure **45** relative to *anti* (*endo*) approach via **46**. There are minor differences in the S−N−C−O dihedral angles (145 v 164°), but overlaying the two transition structures shows a high skeletal superposition.

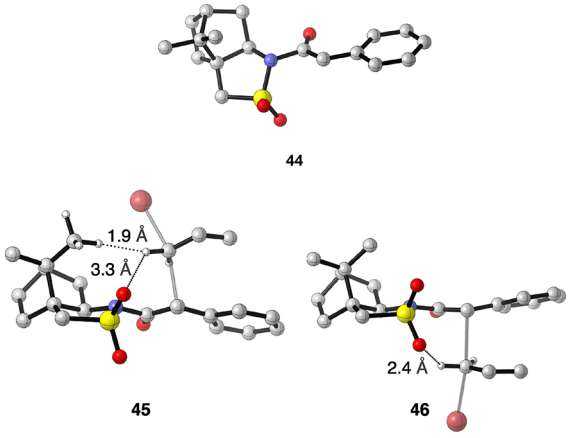

We consider five possible stereochemical determinants emanating from potentially key van der Waals interactions and several critical dihedral angles and distortions within the substrate.

(1) On inspection of **45** and **46**, one is struck by the absence of significant alkyl halide−methyl interactions that are central to all qualitative stereochemical models. The most consequential is a 1.9 Å H−H interaction on *preferred* transition structure **45**. A 2.4 Å H−O contact with the *endo* sulfonyl oxygen in **46** compared to a 3.3 Å H−O contact with the *exo* sulfonyl oxygen in **45** could, in principle, be important, although even 2.4 Å seems distant. We return to this after exploring other contributions.

(2) The alignment of the allyl moieties over the enolate and aromatic ring in **45** and **46** (π-stacking)[60] was found to be stabilizing by approx. 2.0 kcal/mol by comparing isomeric transition structures in which the allyl group is rotated away. Nonetheless, the stereochemical preference is largely retained (2.2 kcal/mol) in the non-π-stacked analogs. Eliminating the π-stacking altogether by replacing the phenyl moiety with a methyl group retains a 2.8 kcal/mol stereochemical preference. Similarly, using methyl bromide instead of allyl bromide shows disparate H−O contacts (3.3 and 2.1 Å) and retains a 2.0 kcal/mol preference for **47** relative to **48**. We switched focus to methylation to simplify subsequent calculations.

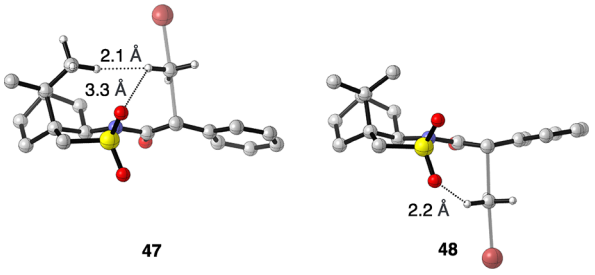

(3) The role of the camphor methyl group in conventional stereochemical models is to block the *exo* face. Removal of the two camphor methyls (see **49** and **50**) shows only a slightly lower (1.4 kcal/mol) facial preference. The desmethyl transition structures **49** and **50**, however, show distortion of the camphor portion accompanied by little change of the S−N−C−O and C−C−C−N dihedral angles.

https://doi.org/10.1021/jacs.2c09341
J. Am. Chem. Soc. XXXX, XXX, XXX−XXX

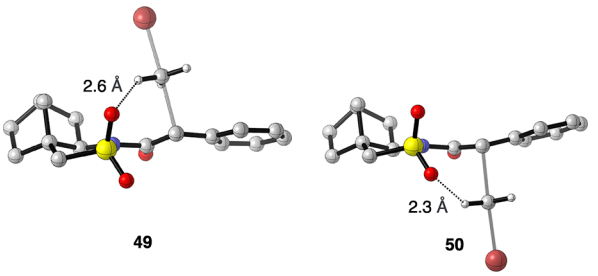

49 50

(4) Given the potentially (but weakly) destabilizing 2.4 Å O−H interaction in **46** and the inconsequential 3.3 Å O−H interaction in **45**, we wondered if the role of the bicyclo[2.2.1] portion of camphor was to influence the sultam conformation. Transition structures **51** and **52** containing only the core sultam ring showed a markedly reduced stereoselectivity (0.4 kcal/mol) accompanied by near parity (2.5 and 2.4 Å, respectively) of the H−O interactions. What was also noticeable, however, is that the C−C−C−N dihedral angles of −41 and −38°, respectively, were reduced when compared to **47** and **48** (−34 and −32°, respectively), causing the sultam to be less puckered. Anchoring the dihedral angles of **51** and **52** to the values observed in **47** and **48** restored the stereochemical preference (1.4 kcal/mol).

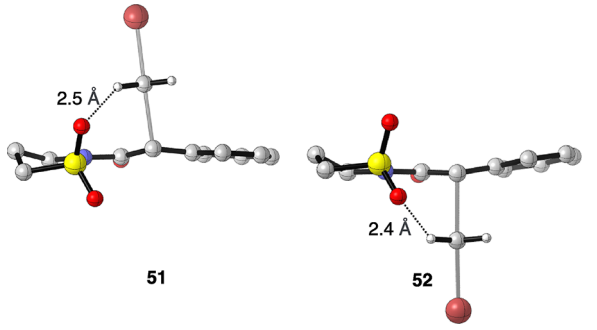

51 52

(5) The emerging model based on an H−O interaction between the alkyl bromide and sulfonyl moiety is appealing, but so was the model based on chelates. It seemed possible that a stereoelectronic effect was at play in which the electrophile preferentially approaches *anti* to the *endo* sulfonyl oxygen as illustrated in **51**. To address this, we removed any possibility of an H−O interaction and dramatically reduced all steric effects by examining proton transfers. After probing a few electrophiles trying to minimize additional unwanted variables, we settled on the metalation of CHF_3 via **53** and **54**. The 1.2 kcal/mol preference for **53** suggests a dominant stereoelectronic influence.

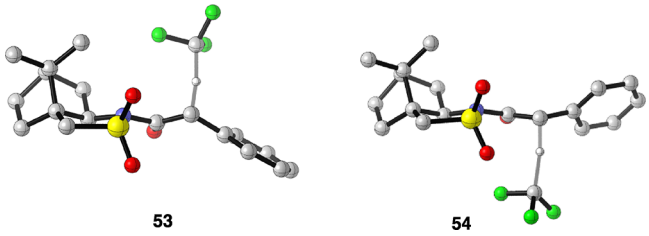

53 54

We must confess that the camphor methyl moiety ostensibly hovering over the face of the enolate always appeared too distant to us, but the universally accepted model was compelling. It appears that the role of the camphor core is to impart chirality and conformational rigidity in the sultam but it offers little in the way of direct van der Waals influence on the incoming electrophile. In short, the stereocontrol emanates from interactions of the electrophile with the sulfonyl, not the camphor core, and even this interaction appears to be stereoelectronic rather than steric.

This stereochemical model reduces Oppolzer enolates to a chiral sultams without a chelate or even a counterion. The results evoke images of alternative applications of sultam-derived enolates of general structure **55**. Alas, there are many substituted sultams, but all are expensive. In this sense, Oppolzer's auxiliary is uniquely suited for the task.

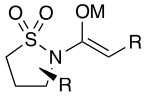

55

CONCLUSIONS

The work described herein began with a seemingly straightforward goal to fill in structural and mechanistic puzzle pieces in the story of stereoselective enolate alkylation. It is commonplace for the complexity and unanticipated results to exceed our expectations, but we continue to be surprised. The structural studies proved quite complex and challenging; enolates have generally proven far more difficult to study than, for example, lithium amides.

For those interested in solvation, we should underscore the value of kinetics to study primary- *and* secondary-shell solvation. The high HMPA order is not surprising: HMPA is reputed to solvate and ionize lithium salts. The medium effects in which toluene stabilizes the ground state and THF stabilizes the transition state are quite surprising. Although they may appear to be purely academic on first inspection, there are potential practical consequences. A 10-fold rate inhibition by the "inert" cosolvent toluene could impose considerable cost differences as process chemists choose between heptane and toluene. To unquestioningly treat these two solvents as interchangeable in *any* setting would be a mistake.

It is dangerous to extrapolate or generalize the results from a single detailed mechanistic study, but there is a case for rethinking all reactions of the Oppolzer auxiliary. Given the irrelevance of the solvent-separated counterion, alkylations of the sodium enolates generated from NaHMDS/THF might also follow this same model. Oppolzer enolates with alternative counterions such as zinc, titanium, or boron could proceed by open transition structures as found in boron variants of Evans enolates with the sultam rather than the camphor methyl moiety still dictating the stereoselectivity. Could 1,4-additions and Diels−Alder cycloadditions to unsaturated Oppolzer sultams also be under the influence of stereoelectronic control by the sultam ring? The complete story makes us wonder if stereoelectronic effects of sulfonyl and other S(IV) and S(VI) moieties on stereocontrolled functionalizations might be overlooked.

The ionization-based mechanism suggests that those looking for alternatives to HMPA should be pondering lithium-ion-selective ligands. Of course, synthetic chemists turned to sodium enolates, probably paying little or no attention to the counterion's role. We already have preliminary data showing that sodiated Oppolzer enolates are challenging to study, but that is another story altogether.

EXPERIMENTAL SECTION

Reagents and Solvents. LDA, [^{6}Li]LDA, and [^{6}Li,^{15}N]LDA were prepared as white crystalline solids.[61] Toluene, hexanes, THF, MTBE, cyclopentane, 2,5-Me_2THF, and HMPA were distilled from

https://doi.org/10.1021/jacs.2c09341
J. Am. Chem. Soc. XXXX, XXX, XXX−XXX

blue or purple solutions containing sodium benzophenone ketyl. Allyl bromide was distilled from 4 Å molecular sieves. Substrates **7a**–**u** were prepared according to slightly modified literature procedures.[9]

Synthesis of [^{15}N]Camphorsulfonamide. [^{15}N]camphorsulfonyl chloride was prepared by adding thionyl chloride ($SOCl_2$, 1.45 mL, 20.0 mmol) and 2 drops of *N*,*N*-dimethylformamide (DMF) to solid camphorsulfonic acid (3.1 g, 13.3 mmol) at room temperature. The slurry was stirred at 90 °C until gas generation ceased. Meanwhile, [^{15}N]NH_3 was generated from [^{15}N]NH_4Cl (>99% ^{15}N isotopic purity, 1.3 g, 23.9 mmol) and excess solid NaOH.[62] The resulting [^{15}N]NH_3 (approx. 0.6 mL) was dissolved in 1.0 mL of water and added to the camphorsulfonyl chloride on ice with vigorous stirring. Note: This reaction is highly exothermic. Water (5.0 mL) was added to the reaction. The reaction was allowed to warm to room temperature over several hours and tracked by TLC (SiO_2, 1:1 Hex/EtOAc). The insoluble [^{15}N]camphorsulfonamide (1.3 g, 42.5%) was collected by filtration, dried *in vacuo*, and used without further purification. [^{15}N]camphorsultam was prepared from [^{15}N]camphorsulfonamide according to literature procedures.[63,64] ^{1}H NMR (500 MHz, $CDCl_3$) δ 5.34 (d, J = 78.2 Hz, 2H), 3.47 (d, J = 15.1 Hz, 1H), 3.13 (d, J = 15.1 Hz, 1H), 2.43 (ddd, J = 18.8, 5.0, 2.7 Hz, 1H), 2.16 (dd, J = 8.1, 3.5 Hz, 2H), 2.11–2.02 (m, 2H), 1.96 (d, J = 18.7 Hz, 1H), 1.52–1.43 (m, 1H), 1.01 (s, 3H), 0.93 (s, 3H). ^{13}C NMR (126 MHz, $CDCl_3$) δ 217.81, 59.53, 54.21, 54.19, 49.27, 43.23, 42.98, 27.21, 26.99, 20.12, 19.53. ^{15}N NMR (61 MHz, $CDCl_3$) δ 97.30. HRMS (DART) Calc. for $C_{10}H_{18}{}^{15}NO_3S^+$ ($M + H^+$): 233.09723; found: 233.09855.

NMR Spectroscopic Analyses. An NMR tube fitted with a double-septum under vacuum was flame-dried on a Schlenk line, allowed to passively cool to room temperature, backfilled with argon, and placed in a dry ice/acetone cooling bath. Individual stock solutions of the *N*-acyl sultams and [^{6}Li]LDA were prepared at room temperature and −78 °C, respectively. The appropriate amounts of the *N*-acyl sultams, [^{6}Li]LDA, solvent, and (when applicable) cosolvent were added sequentially via a gastight syringe. The tube was flame-sealed under a partial vacuum while cold to minimize evaporation. The tubes were mixed on a vortex mixer and stored at −80 °C. Unless otherwise stated, all tubes were sealed with a total enolate concentration of 0.10 M. Standard ^{1}H, ^{19}F, ^{6}Li, ^{13}C, ^{15}N, and ^{31}P direct detection spectra were recorded on a 11.8 T spectrometer at 500.1, 470.6, 73.6, 125.8, 50.7, and 202.5 MHz, respectively. ^{1}H, ^{13}C, ^{15}N, and ^{31}P resonances are referenced to their respective standards (Me_4Si, NH_3, and H_3PO_4, all at 0.0 ppm). ^{6}Li resonances are referenced to 0.30 M [^{6}Li]LiCl/MeOH (0.0 ppm). ^{19}F spectra are referenced to C_6H_5F (−113.15 ppm). For quantitated ^{6}Li and ^{19}F spectra, the spin–lattice relaxation (T1) was determined by standard inversion recovery experiments on several samples. The relaxation delay (d1) was set to seven times the average relaxation lifetime. Integration of the NMR signals was determined using the line-fitting method included in MNova (Mestrelab Research S.L.).

Rate Studies. IR spectra were recorded with an in situ IR spectrometer fitted with a 30-bounce, silicon-tipped probe. The spectra were acquired at a gain of 1 and a resolution of 4 cm^{-1}. All tracked reactions were conducted under a positive pressure of argon from a Schlenk line. A representative reaction was carried out as follows: The IR probe was inserted through a Teflon adapter and O-ring seal into an oven-dried cylindrical flask fitted with a magnetic stir bar and a T-joint. The T-joint was capped with a septum for injections and an argon line. After evacuation under full vacuum, heating, and flushing with argon, the flask was charged with the THF/cosolvent mixture of choice (toluene, 2,5-Me_2THF, toluene/cyclopentane) and cooled to −78 °C in a dry ice–acetone bath. A set of 256 baseline scans were collected, and IR spectra were recorded every 15 s from 30 scans. The reaction vessel was charged to 0.025 M **7o** (1704 cm^{-1}). A 2.00 M stock solution of LDA was injected (0.030 M, 1.2 equiv) through the septum, and enolization was tracked to completion (1616 cm^{-1}), typically ∼10 min. Following full disappearance of **7o**, HMPA was added to the reaction as a 4.70 M (75 *v*/*v*%) stock solution in toluene. The reaction was left to stir for another 10 min. At this point, spectral collection was halted, and an additional 256 baseline scans were collected. The spectrometer was configured to collect spectra every 5 s from 16 scans. One set of scans was collected before addition of *neat* allyl bromide through the septum. The reaction was tracked over five half-lives monitoring the disappearance of the enolate (1616 cm^{-1}) and appearance of the allyl adduct (1706 cm^{-1}).

Single Crystal X-ray Diffraction. Low-temperature X-ray diffraction data were collected on a Rigaku XtaLAB Synergy diffractometer coupled to a Rigaku Hypix detector with Cu Kα radiation (λ = 1.54184 Å) from a PhotonJet microfocus X-ray source at 100 K. The diffraction images were processed and scaled using the CrysAlisPro software.[65] The structures were solved through intrinsic phasing using SHELXT[66] and refined against F^2 on all data by full-matrix least squares with SHELXL[67] following established refinement strategies.[68] All non-hydrogen atoms were refined anisotropically. All hydrogen atoms bound to carbon were included in the model at geometrically calculated positions and refined using a riding model. The isotropic displacement parameters of all hydrogen atoms were fixed to 1.2 times the Ueq value of the atoms they are linked to (1.5 times for methyl groups).

Structures for dimer **22** and dianion **33** were refined as inversion twins. Both structures **22** and **33** contain disordered solvent molecules of THF that were included in the unit cell but could not be satisfactorily modeled. Therefore, those solvents were treated as diffuse contributions to the overall scattering without specific atom positions using the solvent mask routine in Olex2.[69] Details of the crystal growth conditions, data quality, and a summary of the residual values of the refinements are available in the Supporting Information.

Density Functional Theory (DFT) Computations. All DFT calculations were carried out using Gaussian 16.[26] Prompted by a recent benchmarking of modern density functionals, all calculations were conducted at the M06-2X level of theory using Grimme's zero-dampened DFT-D3 dispersion corrections.[27a–d] A pruned (99, 590) integration grid (equivalent to Gaussian's "UltraFine" option) was used for all calculations. Where appropriate, solvation effects were accounted for by the Self Consistent Reaction Field method using the SMD model of Truhlar and coworkers.[27e] Jensen's polarization-consistent segment-contracted basis set, pcseg-1, was used for geometry optimizations, and the expanded pcseg-2 basis set was used for single-point energy calculations.[27f] Basis set files were obtained from the Basis Set Exchange.[27g] Ball-and-stick models were rendered using CYLview 1.0b.[27h] A large number of DFT-computed energies are archived in the Supporting Information.[28]

■ ASSOCIATED CONTENT

Supporting Information

The Supporting Information is available free of charge at https://pubs.acs.org/doi/10.1021/jacs.2c09341.

Synthetic and experimental procedures and spectroscopic, rate, diffraction, and computational data (PDF)

Accession Codes

CCDC 2202043–2202046 contain the supplementary crystallographic data for this paper. These data can be obtained free of charge via www.ccdc.cam.ac.uk/data_request/cif, or by emailing data_request@ccdc.cam.ac.uk, or by contacting The Cambridge Crystallographic Data Centre, 12 Union Road, Cambridge CB2 1EZ, UK; fax: +44 1223 336033.

■ AUTHOR INFORMATION

Corresponding Author

David B. Collum − *Department of Chemistry and Chemical Biology Baker Laboratory, Cornell University Ithaca, New York 14853-1301, United States;* orcid.org/0000-0001-6065-1655; Email: dbc6@cornell.edu

https://doi.org/10.1021/jacs.2c09341
J. Am. Chem. Soc. XXXX, XXX, XXX−XXX

Authors

Nathan M. Lui − *Department of Chemistry and Chemical Biology Baker Laboratory, Cornell University Ithaca, New York 14853-1301, United States;* orcid.org/0000-0003-4950-0914

Samantha N. MacMillan − *Department of Chemistry and Chemical Biology Baker Laboratory, Cornell University Ithaca, New York 14853-1301, United States;* orcid.org/0000-0001-6516-1823

Complete contact information is available at: https://pubs.acs.org/10.1021/jacs.2c09341

Notes

The authors declare no competing financial interest.

■ ACKNOWLEDGMENTS

We thank the National Institutes of Health (GM131713) for support. This work made use of the Cornell University NMR Facility, which is supported, in part, by the National Science Foundation through MRI award CHE-1531632. N.M.L. thanks the Cornell glass shop.

■ REFERENCES

(1) Dugger, R. W.; Ragan, J. A.; Ripin, D. H. B. Survey of GMP Bulk Reactions Run in a Research Facility Between 1985 and 2002. *Org. Process Res. Dev.* **2005**, *9*, 253.

(2) For applications of lithium enolates in pharmaceutical chemistry, see (a) Farina, V.; Reeves, J. T.; Senanayake, C. H.; Song, J. J. Asymmetric Synthesis of Active Pharmaceutical Ingredients. *Chem. Rev.* **2006**, *106*, 2734. (b) Wu, G.; Huang, M. Organolithium Reagents in Pharmaceutical Asymmetric Processes. *Chem. Rev.* **2006**, *106*, 2596. (c) Rathman, T. L.; Bailey, W. F. Optimization of Organolithium Reactions. *Org. Process Res. Dev.* **2009**, *13*, 144.

(3) A survey of approximately 700 total syntheses compiled by H. J. Reich and co-workers revealed LDA to be the most commonly used reagent. The database currently resides at: The Hans Reich's Collection. https://organicchemistrydata.org/hansreich/resources/syntheses/?index=groupby%2Finformation&page=acknowledgment%2F (accessed 2021-10-23).

(4) For reviews of enolates in synthesis, see (a) Green, J. R. In *Science of Synthesis*; Georg Thieme Verlag: New York, 2005; Vol. *8a*, pp. 427−486. (b) Schetter, B.; Mahrwald, R. Modern Aldol Methods for the Total Synthesis of Polyketides. *Angew. Chem., Int. Ed.* **2006**, *45*, 7506. (c) Braun, M. Lithium Enolates: 'Capricious' Structures - Reliable Reagents for Synthesis. *Helv. Chim. Acta* **2015**, *98*, 1. (d) Also, see refs 2a and 2b.

(5) (a) McNeil, A. J.; Toombes, G. E. S.; Chandramouli, S. V.; Vanasse, B. J.; Ayers, T. A.; O'Brien, M. K.; Lobkovsky, E.; Gruner, S. M.; Marohn, J. A.; Collum, D. B. Characterization of β-Amino Ester Enolates as Hexamers via ^{6}Li NMR Spectroscopy. *J. Am. Chem. Soc.* **2004**, *126*, 5938. (b) Liou, L. R.; McNeil, A. J.; Toombes, G. E. S.; Collum, D. B. Structures of β-Amino Ester Enolates: New Strategies Using the Method of Continuous Variation. *J. Am. Chem. Soc.* **2008**, *130*, 17334.

(6) Liou, L. R.; McNeil, A. J.; Ramírez, A.; Toombes, G. E. S.; Gruver, J. M.; Collum, D. B. Lithium Enolates of Simple Ketones: Structure Determination Using the Method of Continuous Variation. *J. Am. Chem. Soc.* **2008**, *130*, 4859.

(7) Renny, J. S.; Tomasevich, L. L.; Tallmadge, E. H.; Collum, D. B. Method of Continuous Variations: Applications of Job Plots to the Study of Molecular Associations in Organometallic Chemistry. *Angew. Chem., Int. Ed.* **2013**, *52*, 11998.

(8) By compound number: (a) **2**: Jin, K. J.; Collum, D. B. Solid-State and Solution Structures of Glycinimine-Derived Lithium Enolates. *J. Am. Chem. Soc.* **2015**, *137*, 14446. (b) **3**: Houghton, M. J.; Collum, D. B. Lithium Enolates Derived from Weinreb Amides: Insights into Five-Membered Chelate Rings. *J. Org. Chem.* **2016**, *81*, 11057. (c) **4**: Houghton, M. J.; Biok, N. A.; Huck, C. J.; Algera, R. F.; Keresztes, I.; Wright, S. W.; Collum, D. B. Lithium Enolates Derived from Pyroglutaminol: Aggregation, Solvation, and Atropisomerism. *J. Org. Chem.* **2016**, *81*, 4149. (d) **5**: Tallmadge, E. H.; Collum, D. B. Evans Enolates: Solution Structures of Lithiated Oxazolidinone-Derived Enolates. *J. Am. Chem. Soc.* **2015**, *137*, 13087. (e) **6** (M = Li): Zhou, Y.; Jermaks, J.; Keresztes, I.; MacMillan, S. N.; Collum, D. B. Pseudoephedrine-Derived Myers Enolates: Structures and Influence of Lithium Chloride on Reactivity and Mechanism. *J. Am. Chem. Soc.* **2019**, *141*, 5444. (f) **6** (M = Na): Zhou, Y.; Keresztes, I.; MacMillan, S. N.; Collum, D. B. Disodium Salts of Pseudoephedrine-Derived Myers Enolates: Stereoselectivity and Mechanism of Alkylation. *J. Am. Chem. Soc.* **2019**, *141*, 16865.

(9) (a) Oppolzer, W. Camphor Derivatives as Chiral Auxiliaries in Asymmetric Synthesis. *Tetrahedron* **1987**, *43*, 1969. (b) Heravi, M. M.; Zadsirjan, V. Recent Advances in the Application of the Oppolzer Camphorsultam as a Chiral Auxiliary. *Tetrahedron: Asymmetry* **2014**, *25*, 1061.

(10) Yang, C.; Sheng, X.; Zhang, L.; Yu, J.; Huang, D. Arylacetic Acids in Organic Synthesis. *Asian J. Org. Chem.* **2020**, *9*, 23.

(11) Gouda, A. M.; Beshr, E. A.; Almalki, F. A.; Halawah, H. H.; Taj, B. F.; Alnafaei, A. F.; Alharazi, R. S.; Kazi, W. M.; AlMatrafi, M. M. Arylpropionic Acid-Derived NSAIDs: New Insights on Derivatization, Anticancer Activity and Potential Mechanism of Action. *Bioorg. Chem.* **2019**, *92*, 103224.

(12) (a) Oppolzer, W.; Tamura, O. Asymmetric Synthesis of α-Amino Acids and α-N-Hydroxyamino Acids via Electrophilic Amination of Bornanesultam-Derived Enolates with 1-Chloro-1-Nitrosocyclohexane. *Tetrahedron Lett.* **1990**, *31*, 991. (b) Oppolzer, W.; Tamura, O.; Deerberg, J. Asymmetric Synthesis of α-Amino Acid and α-*N*-Hydroxyamino Acids from *N*-Acylbornane-10,2-Sultams: 1-Chloro-1-Nitrosocyclohexane as a Practical [NH] Equivalent. *Helv. Chim. Acta* **1992**, *75*, 1965. (c) Oppolzer, W.; Darcel, C.; Rochet, P.; Rosset, S.; De Brabander, J. Non-Destructive Removal of the Bornanesultam Auxiliary in α-Substituted *N*-Acylbornane-10,2-Sultams under Mild Conditions: An Efficient Synthesis of Enantiomerically Pure Ketones and Aldehydes. *Helv. Chim. Acta* **1997**, *80*, 1319. (d) Lu, W. C.; Cao, X. F.; Hu, M.; Li, F.; Yu, G. A.; Liu, S. H. A Highly Enantioselective Access to Chiral 1-(β-Arylalkyl)-1H-1,2,4- Triazole Derivatives as Potential Agricultural Bactericides. *Chem. Biodiversity* **2011**, *8*, 1497.

(13) Edwards, J. O.; Greene, E. F.; Ross, J. From Stoichiometry and Rate Law to Mechanism. *J. Chem. Educ.* **1968**, *45*, 381.

(14) (a) Seebach, D. Structure and Reactivity of Lithium Enolates. From Pinacolone to Selective C-Alkylations of Peptides. Difficulties and Opportunities Afforded by Complex Structures. *Angew. Chem., Int. Ed. Engl.* **1988**, *27*, 1624. (b) Structural studies of enolates: Williard, P. G. In *Comprehensive Organic Synthesis*; Pergamon: New York, 1991. (c) Also, see ref 4e.

(15) (a) Günther, H. Selected Topics from Recent NMR Studies of Organolithium Compounds. *J. Braz. Chem. Soc.* **1999**, *10*, 241. (b) Reich, H. J. Role of Organolithium Aggregates and Mixed Aggregates in Organolithium Mechanisms. *Chem. Rev.* **2013**, *113*, 7130.

(16) Lucht, B. L.; Collum, D. B. Lithium Hexamethyldisilazide: A View of Lithium Ion Solvation Through a Glass-Bottom Boat. *Acc. Chem. Res.* **1999**, *32*, 1035.

(17) Extensive leading references to structural studies of lithium enolates are provided in ref 6.

(18) For examples of colligative measurements on lithium enolates, see (a) Bauer, W.; Seebach, D. Bestimmung des Aggregationsgrads lithiumorganischer Verbindungen durch Kryoskopie in Tetrahydrofuran. *Helv. Chim. Acta* **1984**, *67*, 1972. (b) Arnett, E. M.; Moe, K. D. Proton Affinities and Aggregation States of Lithium Alkoxides, Phenolates, Enolates, β-Dicarbonyl Enolates, Carboxylates, and Amidates in Tetrahydrofuran. *J. Am. Chem. Soc.* **1991**, *113*, 7288. (c) Arnett, E. M.; Fisher, F. J.; Nichols, M. A.; Ribeiro, A. A.

Structure-Energy Relations for the Aldol Reaction in Nonpolar Media. *J. Am. Chem. Soc.* **1990**, *112*, 801.
(19) Guang, J.; Liu, Q. P.; Hopson, R.; Williard, P. G. Lithium Pinacolone Enolate Solvated by Hexamethylphosphoramide. *J. Am. Chem. Soc.* **2015**, *137*, 7347.
(20) Neufeld, R.; Stalke, D. Accurate Molecular Weight Determination of Small Molecules *via* DOSY-NMR by Using External Calibration Curves with Normalized Diffusion Coefficients. *Chem. Sci.* **2015**, *6*, 3354.
(21) Algera, R. F.; Ma, Y.; Collum, D. B. Sodium Diisopropylamide: Aggregation, Solvation, and Stability. *J. Am. Chem. Soc.* **2017**, *139*, 7921.
(22) Williard explicitly uses DOSY to study solvation: Tai, O.; Hopson, R.; Williard, P. G. Ligand Binding Constants to Lithium Hexamethyldisilazide Determined by Diffusion-Ordered NMR Spectroscopy. *J. Org. Chem.* **2017**, *82*, 6223.
(23) (a) Jermaks, J.; Tallmadge, E. H.; Keresztes, I.; Collum, D. B. Lithium Amino Alkoxide-Evans Enolate Mixed Aggregates: Aldol Addition with Matched and Mismatched Stereocontrol. *J. Am. Chem. Soc.* **2018**, *140*, 3077. (b) Sott, R.; Granander, J.; Hilmersson, G. Solvent-Dependent Mixed Complex Formation—NMR Studies and Asymmetric Addition Reactions of Lithioacetonitrile to Benzaldehyde Mediated by Chiral Lithium Amides. *Chem. − Eur. J.* **2002**, *8*, 2081. (c) Jacobson, M. A.; Keresztes, I.; Williard, P. G. On the Mechanism of THF Catalyzed Vinylic Lithiation of Allylamine Derivatives: Structural Studies Using 2-D and Diffusion-Ordered NMR Spectroscopy. *J. Am. Chem. Soc.* **2005**, *127*, 4965. (d) Also, see ref 8f.
(24) The *intended* mole fraction refers to the mole fraction based on what was added to the samples. The *measured* mole fraction—the mole fraction within only the ensemble of interest—eliminates the distorting effects of impurities.
(25) Slow aggregate equilibration for even simple enolates at −78 °C is a phenomenon with potentially significant consequences[8a,d,e] that may be underappreciated by many practitioners.
(26) Frisch, M. J.; Trucks, G. W.; Schlegel, H. B.; Scuseria, G. E.; Robb, M. A.; Cheeseman, J. R.; Scalmani, G.; Barone, V.; Petersson, G. A.; Nakatsuji, H.; Li, X.; Caricato, M.; Marenich, A. V.; Bloino, J.; Janesko, B. G.; Gomperts, R.; Mennucci, B.; Hratchian, H. P.; Ortiz, J. V.; Izmaylov, A. F.; Sonnenberg, J. L.; Williams-Young, D.; Ding, F.; Lipparini, F.; Egidi, F.; Goings, J.; Peng, B.; Petrone, A.; Henderson, T.; Ranasinghe, D.; Zakrzewski, V. G.; Gao, J.; Rega, N.; Zheng, G.; Liang, W.; Hada, M.; Ehara, M.; Toyota, K.; Fukuda, R.; Hasegawa, J.; Ishida, M.; Nakajima, T.; Honda, Y.; Kitao, O.; Nakai, H.; Vreven, T.; Throssell, K.; Montgomery, J. A., Jr.; Peralta, J. E.; Ogliaro, F.; Bearpark, M. J.; Heyd, J. J.; Brothers, E. N.; Kudin, K. N.; Staroverov, V. N.; Keith, T. A.; Kobayashi, R.; Normand, J.; Raghavachari, K.; Rendell, A. P.; Burant, J. C.; Iyengar, S. S.; Tomasi, J.; Cossi, M.; Millam, J. M.; Klene, M.; Adamo, C.; Cammi, R.; Ochterski, J. W.; Martin, R. L.; Morokuma, K.; Farkas, O.; Foresman, J. B.; Fox, D. J. *Gaussian 16, Revision C.01*; Gaussian, Inc.: Wallingford CT, 2016.
(27) (a) Mardirossian, N.; Head-Gordon, M. Thirty Years of Density Functional Theory in Computational Chemistry: An Overview and Extensive Assessment of 200 Density Functionals. *Mol. Phys.* **2017**, *115*, 2315. (b) Wang, Y.; Verma, P.; Jin, X.; Truhlar, D. G.; He, X. Revised M06 Density Functional for Main-Group and Transition-Metal Chemistry. *Proc. Natl. Acad. Sci. U. S. A.* **2018**, *115*, 10257. (c) Zhao, Y.; Truhlar, D. G. The M06 Suite of Density Functionals for Main Group Thermochemistry, Thermochemical Kinetics, Noncovalent Interactions, Excited States, and Transition Elements: Two New Functionals and Systematic Testing of Four M06-Class Functionals and 12 Other Function. *Theor. Chem. Acc.* **2008**, *120*, 215. (d) Grimme, S.; Antony, J.; Ehrlich, S.; Krieg, H. A Consistent and Accurate Ab Initio Parametrization of Density Functional Dispersion Correction (DFT-D) for the 94 Elements H-Pu. *J. Chem. Phys.* **2010**, *132*, 154104. (e) Marenich, A. V.; Cramer, C. J.; Truhlar, D. G. Universal Solvation Model Based on Solute Electron Density and a Continuum Model of the Solvent Defined by the Bulk Dielectric Constant and Atomic Surface Tensions. *J. Phys. Chem. B* **2009**, *113*, 6378. (f) Jensen, F. Unifying General and Segmented Contracted Basis Sets. Segmented Polarization Consistent Basis Sets. *J. Chem. Theory Comput.* **2014**, *10*, 1074. (g) Pritchard, B. P.; Altarawy, D.; Didier, B.; Gibson, T. D.; Windus, T. L. New Basis Set Exchange: An Open, Up-to-Date Resource for the Molecular Sciences Community. *J. Chem. Inf. Model.* **2019**, *59*, 4814. (h) *CYLview, 1.0b*; C. Y., Legault, Université de Sherbrooke 2009 (http://www.cylview.org; accessed 2022-11-17).
(28) For leading references to computations of lithium enolate alkylations, see (a) Ikuta, Y.; Tomoda, S. Origin of Stereochemical Reversal in Meyers-Type Enolate Alkylations. Importance of Intramolecular Li Coordination and Solvent Effects. *Org. Lett.* **2004**, *6*, 189. (b) Elango, M.; Parthasarathi, R.; Subramanian, V.; Chattaraj, P. K. Alkylation of Enolates: An Electrophilicity Perspective. *Int. J. Quantum Chem.* **2006**, *106*, 852. (c) Also, see ref 8.
(29) In general, lower aggregates are promoted by higher steric demands and anion stabilization. High concentrations or strongly coordinating solvents often promote lower aggregates, but sweeping statements about the influence of solvation on aggregation can be misleading.
(30) We did, however, notice a measurable downfield shift in the ^{6}Li resonance of monomeric **8t** with added pyridine, which could be construed as additional cooperative solvation with accompanying cleavage of the chelate.
(31) (a) Tsunoda, T.; Sasaki, O.; Itô, S. Aza-Claisen Rearrangement of Amide Enolates. Stereoselective Synthesis of 2,3-disubstituted Carboxamides. *Tetrahedron Lett.* **1990**, *31*, 727. (b) Kanemasa, S.; Nomura, M.; Yoshinaga, S.; Yamamoto, H. High Enantiocontrol of Michael Additions by Use of 2,2-Dimethyloxazolidine Chiral Auxiliaries. Exclusively *ul,lk*-1,4-Inductive Michael Additions of the Lithium (Z)-Enolate of (S)-4-Benzyl-2,2,5,5-tetramethyl-3-propanoyloxazolidine to *α,β*-Unsaturated Esters. *Tetrahedron* **1995**, *51*, 10463. (c) Manthorpe, J. M.; Gleason, J. L. Stereoselective Generation of E- and Z-Disubstituted Amide Enolates. Reductive Enolate Formation from Bicyclic Thioglycolate Lactams. *J. Am. Chem. Soc.* **2001**, *123*, 2091. (d) Evans, D. A.; Takacs, J. M. Enantioselective Alkylation of Chiral Enolates. *Tetrahedron Lett.* **1980**, *21*, 4233. (e) Evans, D. A.; Bartroli, J.; Shih, T. L. Enantioselective Aldol Condensations. 2. Erythro-Selective Chiral Aldol Condensations via Boron Enolates. *J. Am. Chem. Soc.* **1981**, *103*, 2127.
(32) Reich studied highly fluxional HMPA-solvated organolithiums at cryogenic temperatures below −140 °C. Hardware and solubilities limited us from this type of cryogenic study.
(33) Mixtures of enantiomers using enolate **8t** showed no detectable heterodimer, indicating it either failed to resolve spectroscopically or the two enantiomers do not mix. DFT computations suggest they should mix; we have no further insight or comment.
(34) (a) Bruneau, A. M.; Liou, L.; Collum, D. B. Solution Structures of Lithium Amino Alkoxides Used in Highly Enantioselective 1,2-Additions. *J. Am. Chem. Soc.* **2014**, *136*, 2885. (b) Pöppler, A. C.; Meinholz, M. M.; Faßhuber, H.; Lange, A.; John, M.; Stalke, D. Mixed Crystalline Lithium Organics and Interconversion in Solution. *Organometallics* **2012**, *31*, 42.
(35) Prismatic hexamers with S_6-symmetric cores also show 1:1 subunit ratios.[6]
(36) For leading references to structural studies of dianions, see ref 8e.
(37) (a) Oppolzer, W.; Moretti, R.; Thomi, S. Asymmetric Alkylation of N-Acylsultams: A General Route to Enantiomerically Pure, Crystalline C(*α,α*)-Disubstituted Carboxylic Acid Derivatives. *Tetrahedron Lett.* **1989**, *30*, 5603. (b) Miyabe, H.; Fujii, K.; Naito, T. Radical Addition to Oximeethers for Asymmetric Synthesis of *β*-Amino Acid Derivatives. *Org. Biomol. Chem.* **2003**, *1*, 381.
(38) Several general-purpose reviews on determining reaction mechanism: (a) Meek, S. J.; Pitman, C. L.; Miller, A. J. M. Deducing Reaction Mechanism: A Guide for Students, Researchers, and Instructors. *J. Chem. Educ.* **2016**, *93*, 275. (b) Simmons, E. M.; Hartwig, J. F. On the Interpretation of Deuterium Kinetic Isotope Effects in C−H Bond Functionalizations by Transition Metal Complexes. *Angew. Chem., Int. Ed.* **2012**, *51*, 3066. (c) Collum, D.

https://doi.org/10.1021/jacs.2c09341
J. Am. Chem. Soc. XXXX, XXX, XXX−XXX

B.; McNeil, A. J.; Ramirez, A. Lithium Diisopropylamide: Solution Kinetics and Implications for Organic Synthesis. *Angew. Chem., Int. Ed.* **2007**, *46*, 3002. (d) Algera, R. F.; Gupta, L.; Hoepker, A. C.; Liang, J.; Ma, Y.; Singh, K. J.; Collum, D. B. Lithium Diisopropylamide: Non-Equilibrium Kinetics and Lessons Learned about Rate Limitation. *J. Org. Chem.* **2017**, *82*, 4513.

(39) Singh, K. J.; Hoepker, A. C.; Collum, D. B. Autocatalysis in Lithium Diisopropylamide-Mediated Ortholithiations. *J. Am. Chem. Soc.* **2008**, *130*, 18008.

(40) "[enolate]" refers to the concentration of the monomer subunit (normality). The ligand concentrations in the plots refer to *free* donor solvent concentration.

(41) Rein, A. J.; Donahue, S. M.; Pavlosky, M. A. In Situ FTIR Reaction Analysis of Pharmaceutical-Related Chemistry and Processes. *Curr. Opin. Drug Discovery Dev.* **2000**, *3*, 734.

(42) (a) van't Hoff, J. H.; Cohen, E.; Ewan, T. *Studies in Chemical Dynamics*; Frederik Muller & Co.: Amsterdam, NL, 1896. (b) Upadhyay, S. K. *Chemical Kinetics and Reaction Dynamics; Springer* Netherlands: Dordrecht, NL, 2007.

(43) Ashby, E. C.; Dobbs, F. R.; Hopkins, H. P. Composition of Complex Aluminum Hydrides and Borohydrides, as Inferred from Conductance, Molecular Association, and Spectroscopic Studies. *J. Am. Chem. Soc.* **1973**, *95*, 2823.

(44) The dielectric constants of substituted tetrahydrofurans are slightly lower than THF. (a) Harada, Y.; Salomon, M.; Petrucci, S. Molecular Dynamics and Ionic Associations of Lithium Hexafluoroarsenate ($LiAsF_6$) in 4-Butyrolactone Mixtures with 2-Methyltetrahydrofuran. *J. Phys. Chem.* **1985**, *89*, 2006. (b) Carvajal, C.; Tölle, K. J.; Smid, J.; Szwarc, M. Studies of Solvation Phenomena of Ions and Ion Pairs in Dimethoxyethane and Tetrahydrofuran. *J. Am. Chem. Soc.* **1965**, *87*, 5548.

(45) Aromatic hydrocarbons can markedly alter chemical shifts, aggregation states, and reactivities of organolithiums even in the presence of superior donor solvents. For examples and leading references, see (a) Reyes-Rodríguez, G. J.; Algera, R. F.; Collum, D. B. Lithium Hexamethyldisilazide-Mediated Enolization of Acylated Oxazolidinones: Solvent, Cosolvent, and Isotope Effects on Competing Monomer- and Dimer-Based Pathways. *J. Am. Chem. Soc.* **2017**, *139*, 1233. (b) Godenschwager, P. F.; Collum, D. B. Lithium Hexamethyldisilazide-Mediated Enolizations: Influence of Chelating Ligands and Hydrocarbon Cosolvents on the Rates and Mechanisms. *J. Am. Chem. Soc.* **2007**, *129*, 12023. (c) Lucht, B. L.; Collum, D. B. Lithium Ion Solvation: Amine and Unsaturated Hydrocarbon Solvates of Lithium Hexamethyldisilazide (LiHMDS). *J. Am. Chem. Soc.* **1996**, *118*, 2217. (d) Sun, X.; Collum, D. B. Lithium Diisopropylamide-Mediated Enolizations: Solvent-Independent Rates, Solvent-Dependent Mechanisms. *J. Am. Chem. Soc.* **2000**, *122*, 2452. (e) Chadwick, S. T.; Rennels, R. A.; Rutherford, J. L.; Collum, D. B. Are *n*-BuLi/TMEDA-Mediated Arene Ortholithiations Directed? Substituent-Dependent Rates, Substituent-Independent Mechanisms. *J. Am. Chem. Soc.* **2000**, *122*, 8640.

(46) The allusion to free HMPA is to correct for the decrease in the HMPA concentration owing to the doubly solvated monomer.

(47) Gutmann, V. *The Donor-Acceptor Approach to Molecular Interactions*; Plenum: New York, 1978.

(48) Analogous D_{2d} and S_4 structures are well represented in the Cambridge Crystallographic Database. Groom, C. R.; Bruno, I. J.; Lightfoot, M. P.; Ward, S. C. The Cambridge Structural Database. *Acta Cryst.* **2016**, *B72*, 171.

(49) The A-value of a phenyl moiety—the energy cost of placing it axial on cyclohexane—is 3.1 (kcal/mol), which is substantially larger than secondary alkyl groups. With that said, it is dangerous to use such a specific metric of steric effects for generalized statements.

(50) Pang, H.; Williard, P. G. Solid State Aldol Reactions of Solvated and Unsolvated Lithium Pinacolone Enolate Aggregates. *Tetrahedron* **2020**, *76*, 130913 and references cited therein.

(51) Grabowski, E. J. J. *Reflections on Process Research —The Art of Practical Organic Synthesis*, Abdel-Magid, A. F.; Ragan, J. A., Eds. ACS Symposium Series, 870, American Chemical Society, Washington DC, 2004, *Chapter 1*, pp. 1−21.

(52) (a) Raiser, E. M.; Hauser, C. R. 1,3-Dianion of Dimethyl Sulfone and 1,1-Dianion of Benethyl Phenyl Sulfone. *Tetrahedron Lett.* **1967**, *34*, 3341. (b) Langer, P.; Freiberg, W. Cyclization Reactions of Dianions in Organic Synthesis. *Chem. Rev.* **2004**, *104*, 4125. (c) Fustier-Boutignon, M.; Nebra, N.; Mézailles, N. Geminal Dianions Stabilized by Main Group Elements. *Chem. Rev.* **2019**, *119*, 8555.

(53) In 1983, geminal dianions of general structure $PhSO_2CM_2Ph$ (M = Li, Na, and K) were isolated as solids, and a low-resolution crystal structure of the 1,1-dilithio derivative was obtained: Wanat, R. E.; Collum, D. B., unpublished. A structurally related Ar-$SO_2CLi_2SiMe_3$ analog was eventually published.[54] We treated $PhSO_2CH_3$ with three equiv *n*-BuLi to obtain a solid that provided 2.8 deuteria when quenched with D_2O. An astute colleague recently noted that the possible reductive cleavage of aryl sulfones with tertiary alkyl groups with lithium naphthalide makes this trilithiated derivative a CLi_4 synthon.

(54) Gais, H. J.; Vollhardt, J.; Günther, H.; Moskau, D.; Lindner, H. J.; Braun, S. Solid-State and Solution Structure of Dilithium Trimethyl((Phenylsulfonyl)Methyl)Silane, a True Dilithiomethane Derivative. *J. Am. Chem. Soc.* **1988**, *110*, 978.

(55) Ionization constants for conversion of ion pairs to free ions illustrate the enthalpic contributions of secondary-shell solvation: Hogen-Esch, T. E.; Smid, J. Studies of Contact and Solvent-Separated Ion Pairs of Carbanions. II. Conductivities and Thermodynamics of Dissociation of Fluorenyllithium, −sodium, and −cesium. *J. Am. Chem. Soc.* **1966**, *88*, 318.

(56) Depue, J. S.; Collum, D. B. Structure and Reactivity of Lithium Diphenylamide. Role of Aggregates, Mixed Aggregates, Monomers, and Free Ions on the Rates and Selectivities of *N*-Alkylation and E2 Elimination. *J. Am. Chem. Soc.* **1988**, *110*, 5524.

(57) A marked influence of toluene on LiHMDS-mediated enolizations of oxazolidinones prompted us to conclude that "the toluene effect is most likely a ground-state stabilization."[45a]

(58) We hasten to add that neat toluene becomes *visibly* viscous at −78 °C, which serves as a warning to would-be kineticists. Santos, F. J. V.; de Castro, C. N.; Dymond, J. H. Standard Reference Data for the Viscosity of Toluene. *J. Phys. Chem. Ref. Data* **2006**, *35*, 1.

(59) Ayoub and coworkers pondered the possibility that open transition structures might be involved in the quaternization of a highly stabilized Oppolzer enolates: Ayou, M.; Chassaing, G.; Loffet, A.; Lavielle, S. Diastereoselective Alkylation of Sultam-Derived Amino Acid Aldimines Preparation of Cα-Methylated Amino Acids. *Tetrahedron Lett.* **1995**, *36*, 4069.

(60) (a) Jones, G. B.; Chapman, B. J. π-Stacking Effects in Organic Synthesis. *Synthesis* **1995**, *5*, 475. (b) Mahadevi, A. S.; Sastry, G. N. Cooperativity in Noncovalent Interactions. *Chem. Rev.* **2016**, *116*, 2775.

(61) Ma, Y.; Hoepker, A. C.; Gupta, L.; Faggin, M. F.; Collum, D. B. 1,4-Addition of Lithium Diisopropylamide to Unsaturated Esters: Role of Rate-Limiting Deaggregation, Autocatalysis, Lithium Chloride Catalysis and Other Mixed Aggregation Effects. *J. Am. Chem. Soc.* **2010**, *132*, 15610.

(62) Woltornist, R. A.; Collum, D. B. Aggregation and Solvation of Sodium Hexamethyldisilazide: Across the Solvent Spectrum. *J. Org. Chem.* **2021**, *86*, 2406.

(63) Towson, J. S.; Weismiller, M. C.; Sankar Lal, G.; Sheppard, A. C.; Kumar, A.; Davis, F. A. (+)-(2*R*,8a*S*)-10-(Camphorylsulfonyl)-oxaziridine [4H-4A,7-Methanooxazirino[3,2-*i*][2,1]benzisothiazole, tetrahydro-9,9-dimethyl-, 3,3-dioxide, [4a*S*-(4aα,7α,8a*R**)]]. *Org. Synth.* **1990**, *69*, 158.

(64) Capet, M.; David, F.; Bertin, L.; Hardy, J. C. A Two-Step Synthesis of Camphosultam. *Synth. Commun.* **1995**, *25*, 3323.

(65) *CrysAlisPro*; Rigaku Corporation: The Woodlands, TX, 2015 (https://www.rigaku.com/products/crystallography/crysalis; accessed 2022-11-17).

https://doi.org/10.1021/jacs.2c09341
J. Am. Chem. Soc. XXXX, XXX, XXX−XXX

(66) Sheldrick, G. M. SHELXT - Integrated Space-Group and Crystal-Structure Determination. *Acta Cryst.* **2015**, *71*, 3.
(67) Sheldrick, G. M. A Short History of SHELX. *Acta Cryst.* **2008**, *A64*, 112.
(68) Müller, P. Practical Suggestions for Better Crystal Structures. *Crystallogr. Rev.* **2009**, *15*, 57.
(69) Dolomanov, O. V.; Bourhis, L. J.; Gildea, R. J.; Howard, J. A. K.; Puschmann, H. OLEX2: A Complete Structure Solution, Refinement and Analysis Program. *J. Appl. Crystallogr.* **2009**, *42*, 339.

https://doi.org/10.1021/jacs.2c09341
J. Am. Chem. Soc. XXXX, XXX, XXX−XXX